Pre-normative REsearch for Safe use of Liquid HYdrogen (PRESLHY)

Fuel Cells and Hydrogen Joint Undertaking (FCH JU)

Grant Agreement Number 779613

Deliverable Number:	D2.2
Title:	State of the art analysis
Authors:	Simon Jallais
Submitted Date:	
Due Date:	30 May 2018
Report Classification:	Public

Deliverable	
Contractual delivery date	30 May 2018
Actual delivery date	
Deliverable Number	D2.1
Deliverable Name	State of the art analysis
Internal document ID	D2.2
Nature	Report

Authors		
	Name	Organisation
WP Leader & Coordinator	Simon Jallais	Air Liquide
Participant	Laurence Bernard	Air Liquide
Participant	Alexandros Venetsanos	NCSRD
Participant	Rebecca Lisseman Philip Hooker	HSL
Participant	Mikhail Kuznetsov Thomas Jordan	KIT
Participant	Donatella Cirrone	UU

Disclaimer

Key words

Liquid hydrogen, release, dispersion, fire, explosion, deflagration, detonation, ignition, DDT, jet fire, pool fire, radiation, BLEVE, RPT

Abbreviations

BAM	Bundesanstalt für Materialforschung und -prüfung
barg	Shorthand for gauge pressure in bar
BLEVE	Boiling Liquid Expanding Vapour Explosion
BR	Blockage Ratio
CFD	Computational Fluid Dynamics
CH_4	Methane
DDT	Deflagration to Detonation Transition
DO	Discrete Ordinates
DRIFT	Dispersion of Releases Involving Flammables or Toxics
EDC	Eddy Dissipation Concept
EoS	Equation of State
ESR	Engineering, Safety & Risk
FLACS	Flame Accelerator
GASP	Gas Accumulation over Spreading Pools
GH_2	Gaseous Hydrogen
HEM	Homogeneous Equilibrium Model
HNEM	Homogeneous Non-Equilibrium Model
HSL	Health and Safety Laboratory
INERIS	Institut National de l'Environnement industriel et des Risques
KIT	Karlsruhe Institute of Technology
LFL	Lower Flammable Limit
LH_2	Liquefied Hydrogen
LN_2	Liquefied Nitrogen
LNG	Liquefied Natural Gas
LO_2	Liquefied Oxygen
LPG	Liquefied Petroleum Gas
MIE	Minimum Ignition Energy
N_2	Nitrogen

NASA	National Aeronautics and Space Administration
NIST	National Institute of Standards and Technology
PAICC	Pressure of Adiabatic IsoChoric Combustion
RANS	Reynolds-Averaged Navier-Stokes
RPT	Rapid phase transition
TNO	Toegepast Natuurwetenschappelijk Onderzoek
TNT	Trinitrotoluene
UFL	Upper Flammable Limit
UVCE	Unconfined Vapour Cloud Explosion

Table of Contents

1 Background

The aim of the report is to review the existing literature on physical phenomena associated with liquid hydrogen risks. This literature survey and the PIRT (Phenomena Identification and Ranking Table) planned in September 2018 at the Research Priorities Workshop will be very useful for the refinement of the experimental and modelling program.

2 Release and mixing phenomena

The first step in consequence modelling assessment is the characterisation of the releasesource term and its subsequent mixing with ambient air.

The published experiments are divided in two categories :

- dispersion and pool spreading experiments,
- pressurized release experiments.

2.1 Dispersion and pool spreading experiments (low pressure-large releases)

Previous experimental work is relatively limited and summarised in Table 1 below.

2.1.1 Experiments description

The following figure summarises the main experimental campaigns investigating massive low pressure releases of LH_2.

	Arthur D. Little	NASA	BAM	INERIS (He)	HSL
LH_2 quantity released	5, 120, 2 271 and 18 927 L	5 700 L	650 L	1.5 kg/s 2.1 kg/s	60 L/min (70 g/s)
Spill duration (s)	few seconds	35-85 s	60 & 120 s	30 to 70 s	250 s
Transfer line (m)	No	30	75	> 10	20
Vessel pressure (bar)	no or limited	70 bar by gaseous He	7	not given	2 bara
Ground	Concrete / Soil	steel plate in pond	Aluminium sheet	Metallic plate	Concrete pad

		with sand	Water		
Flow measurements (source term)	no	no	no	yes (storage) weighting)	yes
T ; P at release point	no	no	no	no	only P (1.2 bara)
H_2% measurements	no	yes	yes	yes	yes
Wind conditions measurements	no	yes	no	yes	yes

Figure 1 : Summary of the experimental setups.

The following paragraphs describe the experimental setups and outline the main conclusions.

2.1.2 Arthur D. Little (1960)

Arthur D. Little (1960), under the sponsorship of the US Air Force, performed large LH_2 releases. Tests consisted of 1 ¼, 32, 600 and 5 000 gallons spills (corresponding to 5, 120, 2 271 and 18 927 L) of atmospheric LH_2 on the ground.

For the small-scale tests, LH_2 was stored in Dewar vessels and spilled into pits from the fall of the Dewars on the floor. For the two largest tests, the LH_2 was transferred from a truck to insulated storage which were emptied by opening a bottom valve. For all tests, the cloud remained close to the ground for a few seconds and then gradually rose. For instance, the evaporation of 120 L of LH_2 took 30 seconds.

Unfortunately, the experiments were poorly instrumented for concentrations and/or temperature measurements.

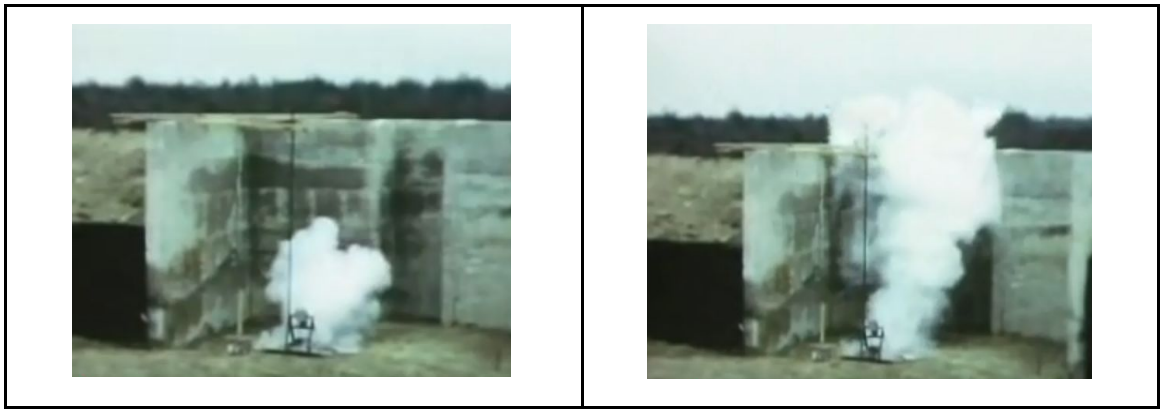

Figure 2 : Photos extracted from the YouTube video (120 L spillage).

The tests also consisted of continuous LH_2 releases (2 L/s over 16 min or 16 L/s over 1 min at wind speed respectively between 1.8 and 7.6 m/s) imitating a pipeline rupture. These experiments revealed a dense visible cloud up to 200 m distance.

Figure 3 : 200 m long cloud formed for the 16 L/min - 1 min experiments.

Interesting videos presenting the experiments are available on Youtube :
https://www.youtube.com/watch?v=7bFJK5kU_UQ
https://www.youtube.com/watch?v=RNzjksIImb8

Reference :
Arthur D. Little Inc. (15.01.1959) Interim Report on an Investigation of Hazards Associated with Liquid Hydrogen Storage and Use.

2.1.3 Zabetakis and Burgess (1961)

Zabetakis and Burgess (1961) determined the evaporation rate of LH_2 from the surface of a block of paraffin wax cast at laboratory scale. They used a 2.8-inch Dewar flask and measured the rates of gas evolution following release of LH_2 into the Dewar. They showed that the vaporization rate of liquid hydrogen can be calculated after the initial period of violent boiling. They then investigated the influence of the ground on the

vaporization rate and spreading of the pool by spilling ~6.8 L of LH_2 from a Dewar on gravel and smooth macadam. The high specific surface of the gravel causes a faster vaporization than the macadam, leading to a higher visible cloud for the same elapsed time.
They also spilled 56 L of LH_2 on smooth steel and gravel surfaces, the cloud was subsequently ignited. The rapid vaporization due to the gravel surface caused the centre of the base of the flame to be closer to the Dewar than observed when using the smooth steel plate.
They also determined experimentally the distribution of flammable volumes from liquid hydrogen spillage from open-mouths Dewar for various quantities of hydrogen from 0.5 to 7.4 L. They tried to correlate the position of the visible cloud to the flammable cloud and found that the visible cloud could not be used as an accurate measure of the position of the flammable zone since the flammable mixtures could be ignited both outside and within the visible cloud

Reference :
Zabetakis, M.G., and Burgess, D.S. (1961) Research on the hazards associated with the production and handling of liquid hydrogen. US Department of the Interior, Bureau of Mines.

2.1.4 NASA (1980)

In 1980, NASA performed large LH_2 spillages in order to assess the scenario of failure of the 3 000 m^3 LH_2 storage tank at the Kennedy Space Center at Cape Canaveral.

Experiments (7 trials) at NASA White Sands consisted in rapid releases near-ground (“compacted sand”) from a 5.7 m^3 of LH_2 with spill durations of approximately 35-85 s. The LH_2 is transferred via a 152 mm inner diameter insulated line of about 30 m length. Prior to the tests, Dewar and line were filled with LH_2. Gaseous Helium was used to pressurise the Dewar to 70 bar before opening the valve at the end of the spill line.

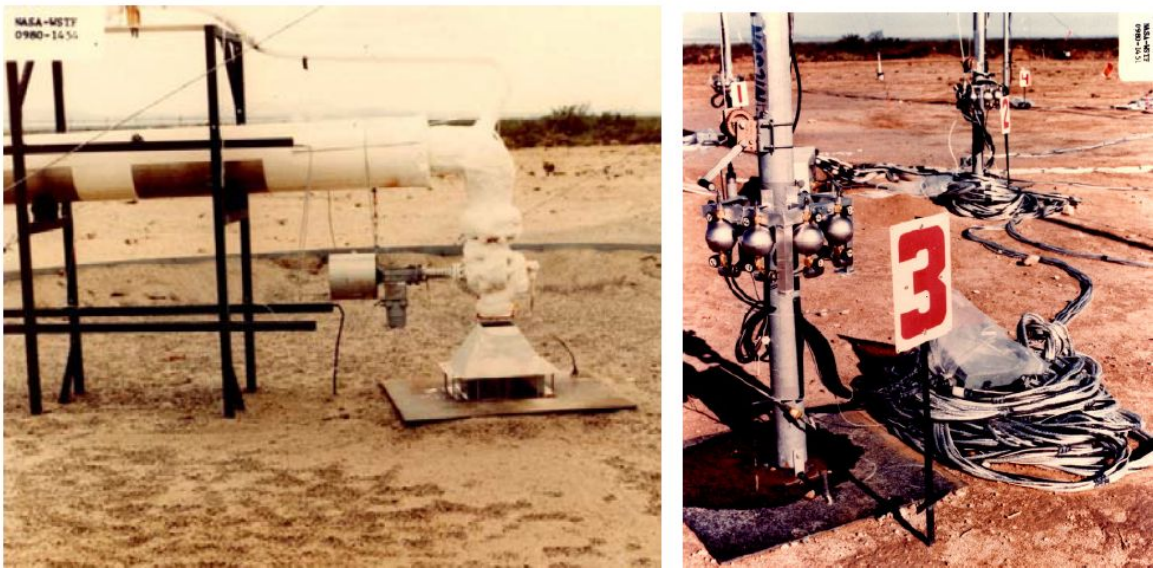

Figure 4 : NASA LH_2 release apparatus.

Instrumented towers, located downwind of the spill site, gathered data on temperature and H_2 concentration as the flammable cloud drifted downwind. Visual phenomena were recorded by motion picture and still cameras.

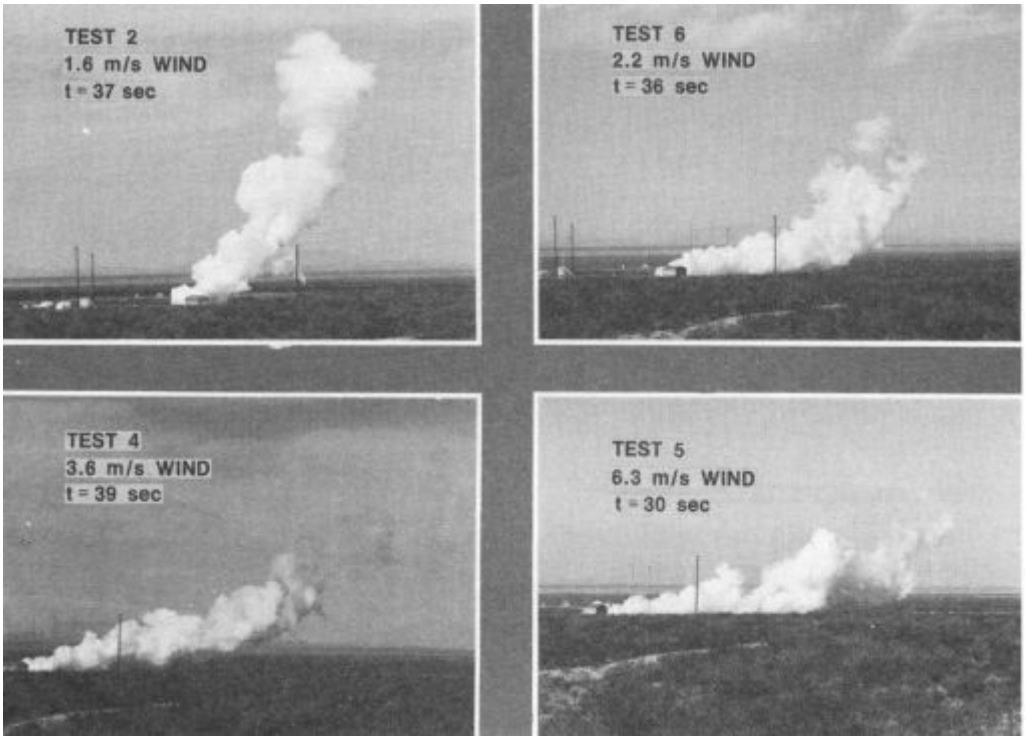

Figure 5 : Photos of the visible cloud for 4 tests

Parameter	Test 1	Test 2	Test 3	Test 4	Test 5	Test 6	Test 7
LH_2 spill quantity [m^3]	5110	5110	5110	5110	2270 - 2650	5110	2840
Spill time [s]	63	39	85	35	15 - 20	38	120
Time to total vaporization [s]	102	57	94	42	29.5	43	-
Visible cloud duration [s]	116	80	-	90	50	90	-
Downwind dist. to flammable cloud [m]	-	152	24	53	27	65	9
H_2 concentration at dew point [%]	9.4	4.5	9.8	4.6	2.6	6.7	7.1
Atmospheric conditions							
Temperature [°C]	30	25	26	19	12.4	15.5	20.5
Pressure [10^2 Pa]	788	787	789	789	785	786	786
Humidity [%]	18	50	27	27	43	29	30
Dew point [°C]	4.0	12.9	2.0	2.9	5.8	-1.7	-0.8
Wind speed [m/s]	3.5	2.0	4.7	3.4	5.9	1.8	4.2
Stability class	unstable	extremely unstable	unstable	unstable	neutral, slightly stable	unstable	neutral

Figure 6 : Experimental details of the NASA experiments.

CFD simulations of the test 6 have been performed by Venetsanos and Bartzis (2007), Middha *et al.* (2011) and recently by Jin *et al.* (2017) and by Jäkel *et al.* (2017), using ADREA-HF, FLACS, ANSYS/Fluent CFD and KFX codes respectively.
Venetsanos and Bartzis (2007) used the dispersed mixture approach along with HEM model for two-phase flow, which assumes that phases share same velocities (homogeneous) and same pressure and temperature (thermodynamic equilibrium).They calculated the phase distribution using Raoult's law for ideal mixtures. Best agreement with limited concentration measurements was found by modeling the source as a jet, accounting for the small fence around the spill and including heat transfer from the ground (*by solving energy equation inside it*).

Jin *et al.* (2017) used the dispersed mixture approach. They assumed thermodynamic equilibrium between phases, but calculated phase distribution by explicit modeling of vaporization rate along with a transport equation for the gas phase. Regarding phase velocities, the homogeneous assumption was not applied and an algebraic slip model was used to find the slip velocity.

Jäkel *et al.* (2017) developed a new multiphase multicomponent CFD model capable of simulating liquid and gaseous distributions.
Middha *et al.* (2011) used a separated phases approach: a pool model for the liquid phase and CFD only for the vapour phase. With this approach, they were able to provide pool spreading predictions in better agreement with experiments compared to Verfondern and Dienhart (2007) who used the LAuV code. The LAuV code is a pool model which accounts for two-dimensional ground energy transport, but does not include CFD for the vapor phase above the pool.

References :
Witcofski, R.D., Chirivella, J.E. (1984) Experimental and analytical analyses of the mechanisms governing the dispersion of flammable clouds formed by liquid hydrogen spills. International Journal of Hydrogen Energy, Vol. 9(5), Pages 425-435.

Witcofski, R.D. (1981) Dispersion of Flammable Clouds Resulting from Large Spills of Liquid Hydrogen. NASA Technical Memorandum 83131.

Venetsanos, A.G., Bartzis, J.G. (2007) CFD modeling of large-scale LH_2 spills in open environment. International Journal of Hydrogen Energy, Vol. 1(13): Pages 2171-7.

Middha, P., Ichard, M., Arntzen, B.J. (2011) Validation of CFD modeling of LH_2 spread and evaporation against large-scale spill experiments. International Journal of Hydrogen Energy Vol. 36(3): 2620-7.

Jin, T., Liu, Y., Wei, J., Wu, M., Lei, G., Chen, H., Lan, Y. (2017) Modeling and analysis of the flammable vapor cloud formed by liquid hydrogen spills. International Journal of Hydrogen Energy Vol. 42: Pages 26762-26770.

Verfondern, K. and Dienhart, B. (2007) Pool Spreading and Vaporization of Liquid Hydrogen. International Journal of Hydrogen Energy, Vol. 32: Pages 2106-2117.

Jäkel et al. (2017) Validation of a 2D multiphase multicomponent CFD model for accidental liquid and gaseous release. ICHS 2017 Hamburg.

2.1.5 Batelle / BAM LH_2 spills experiments (1994)

The experiments were performed by Batelle Ingenieurtechnik for BAM in the frame of the Euro-Quebec-Hydro-Hydrogen-Pilot-Project (Marinescu-Pasoi and Sturm (1994)).

The total release was 650 L (0.8 kg/s in 60 s and 0.4 kg/s in 120 s) simulating a spill in a residential area. They measured pool spreading rates and gas-cloud concentrations. Storage tanks about 75 m away from the release site supplied liquid hydrogen through suitable transfer lines.

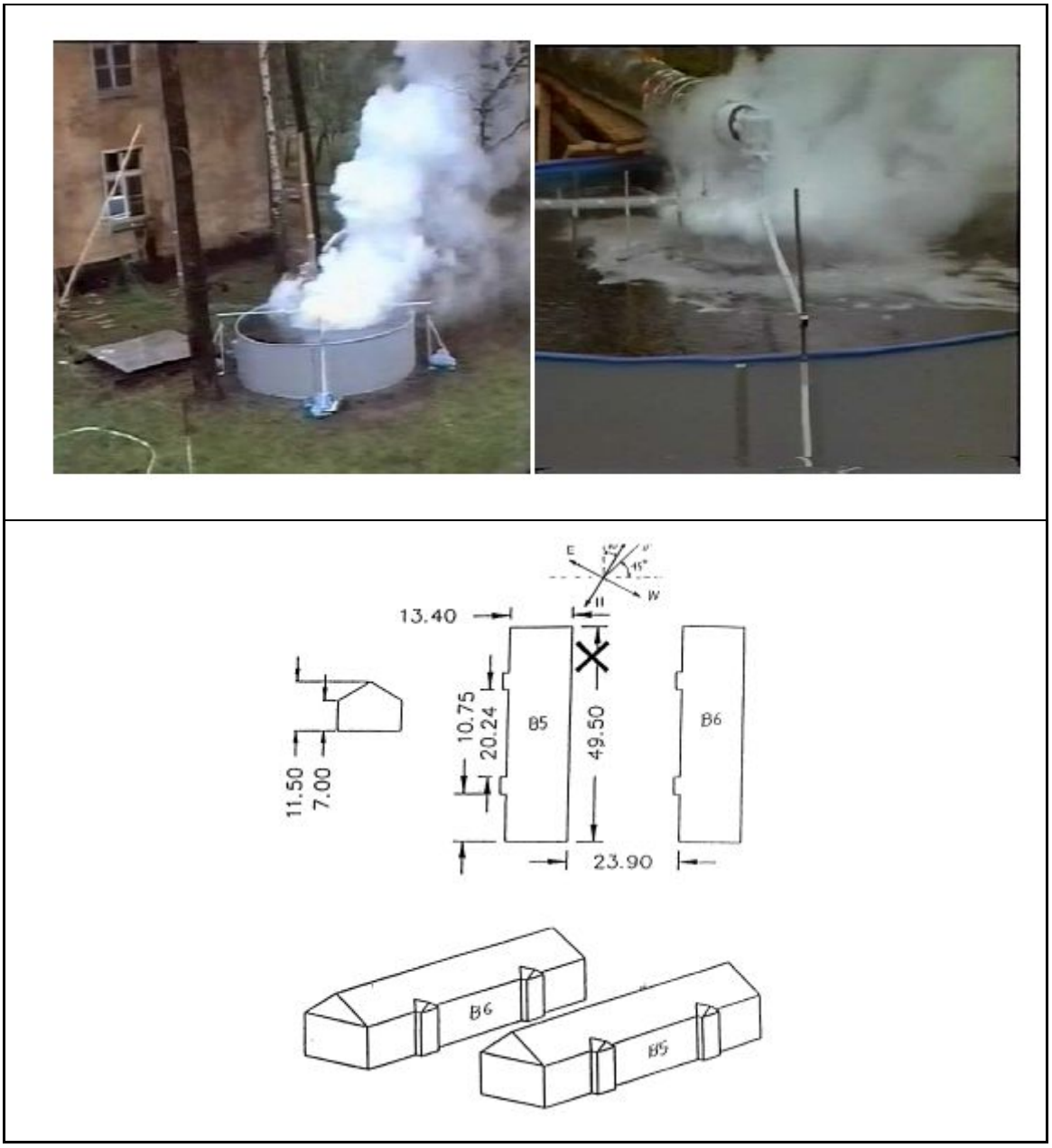

Figure 7 : Pictures and schematics of the BAM experiments.

One set of experiments was dedicated to the dispersion only. The release was performed at different heights above the ground, and the gas came out of the supply line from the pressurized tank with a considerable impulse (average velocity of about 5.6 m/s from a 50 mm i.d. nozzle.) on an aluminium plate of 0.5 m^2. The H_2 measurements corresponding to these data are unfortunately unpublished.

The other set of experiments is dedicated to pool spreading measurements on a water pool (3.6 m diameter) or an aluminium plate (2*2m), (Dienhart, 1995). An impulse-less release (using a diffuser) close to the surface was required. The cryogen hit the surface below the vessel when overflowing the rim. The radius of the LH_2 pool under quasi steady state conditions was about 0.6 m on water and more than 1 m on the aluminium plate. The main difficulty for modelling is the lack of clear definition of the initial conditions: mass fraction of liquid at source point, accurate mass release, atmospheric conditions…

Parameter	Test 1	Test 2	Test 3	Test 4	Test 5	Test 6
Ground	Al sheet (0.5 m^2)	Al sheet (0.5 m^2)	water (9.6 m^2)	water (9.6 m^2)	Al sheet (4 m^2)	Al sheet (4 m^2)
Release time GH_2 [s]	90	30	90	60	60	55
Release time LH_2 [s]	50	61	62	62	62	62
Mass flow [kg/s]	0.315	0.315	0.350	0.350	0.450	0.450
Volume flow [l/s]	4.5	4.5	5	5	6	6
Atmospheric conditions						
Temperature [°C]	12	12	12	12	11	10
Pressure [10^2 Pa]	983	983	985	985	986	986
Humidity [%]	96.5	96.5	96.7	96.7	97.0	97.0
Wind speed [m/s]	0-1	0-1	0-1	0-1	0-1	0-1

Figure 8 : Details of the BAM experiments.

Like their NASA counterparts, BAM researchers concluded that ground heat transfer effects and fast dissipation rates helped limit the size and duration of LH_2 pools and flammable clouds.

Dienhart (1995) pool spreading experiments were successfully simulated using the LAuV code, using shallow layer approach for the pool and a two-dimensional energy equation within the substrate, see also Verfondern, K. and Dienhart, B. (2007). Simulations of pool spreading for NASA-6 experiment resulted in overprediction of the pool radius compared to experimental data (see section on NASA tests above).

Batt (2014) simulated with a reasonable agreement the HSL test 6 and Takeno experiments using the GASP software (Gas Accumulation over Spreading Pools) - developed by ESR in collaboration with the UK HSE and now implemented in the gas dispersion model DRIFT).

References :
Schmidtchen, U., Marinescu-Pasoi, L., Verfondern, K., Nickel, V.; Sturm, B., Dienhart, B. (1994) Simulation of accidental spills of cryogenic hydrogen in a residential area. Cryogenics Vol.34.

Marinescu-Pasoi, L., Sturm, B. (1994) ‘‘Messung der Ausbreitung einer Wasserstoff-und Propanwolke in bebautem Gelaende’’ und ‘‘Gasspezifische Ausbreitungsversuche’’, Battelle Ingenieurtechnik reports R-68202 and R-68264.

Statharas, J.C., Venetsanos, A., Bartzis, J.G., Schmidtchen, U. (2000) Analysis of data from spilling experiments performed with liquid hydrogen. Journal of Hazardous Materials 77(1-3):57-75.

Dienhart, B. (1995) Ausbreitung und Verdampfung von flüssigen Wasserstoff auf wasser und festem Untergrund, Report Jül-3155, Research Center Jülich, Germany.

Verfondern, K. and Dienhart, B. (2007) Pool Spreading and Vaporization of Liquid Hydrogen. International Journal of Hydrogen Energy Vol. 32: 2106-2117.

Verfondern, K. (2007) Safety Considerations on Liquid Hydrogen, Energy & Environment,Vol.10.
(http://juser.fz-juelich.de/record/1311/files/Energie%26Umwelt_10.pdf)

Batt, R. (2014) Modelling of liquid hydrogen spills. RR985 Health Safety Executive.

2.1.6 INERIS Experiments (1995)

In 1995, Proust *et al.* performed large scale dispersion tests with cryogenic helium for its similar dispersion characteristics to liquid hydrogen (temperature, buoyancy). Spillage flow rates of 1.5 kg/s and 2.1 kg/s respectively during several tens of seconds have been investigated. The spillage system consisted of two liquid helium trucks connected to vacuum thermally insulated lines. The physical conditions of the spillage source term are not known (internal flash?, pressure and temperature at orifice?). They measured He concentrations by means of fine thermocouples (more than 130) using an adiabatic mixing assumption. Buoyancy effects including internal turbulence were measured using “bidirectional probes” (5) of Mc Caffrey allowing to determine the cloud velocity and its fluctuations up to the turbulence length scale.

The authors concluded that :
- The size of the cloud depends mainly on the spill flow-rate but marginally on the wind speed;

- The integral scale of turbulence is very close to the size of the lighter zone of the cloud and looks very different from atmospheric turbulence;
- The velocity fluctuations are much larger than in atmospheric turbulence and close in order of magnitude to the upward mean velocity of the plume. This point could have a strong impact in case of delayed ignition.

All these measurements were not integrally published and within the PRESLHY project, they (temperatures, concentrations and velocities) will be provided by INERIS to the partners (modellers and analysts).

Issue n°	duration (s)	Mass flow rate (kg/s)	Wind speed (m/s) at 3 m height	Humidity (%)	Temp (°C)	H1 (m)	H2 (m)	L (m)
0	60	1,5	6	/	16	3	5	20
1	50	1,4	4,0±1,0	86	17	5	17	50
2	52	1,4	5,2±1,0	90	17	5	17	50
3	52	2,1	3,0±0,5	84	12	12	32	80
4	43	2,1	4,0±0,5	84	12	7	35	75
5	34	2,1	5,5±0,5	88	12	7	30	70
6	43	2,1	4,5±0,5	88	11	7	30	70
7	63	1,2	2,0±0,5	85	12			
8	65	1,2	2,0±0,5	85	12			
9	71	2,2	2,0±0,5	85	12			

Figure 9 : Details of INERIS experiments.

References :

Proust, C., Lacome, J.-M., Jamois, D., Perrette, L. (2007) Processes of the formation of large unconfined clouds following a massive spillage of liquid hydrogen on the ground. International Conference on Hydrogen Safety (ICHS 2007), San Sebastian, Spain.

Lacome, J.-M., Proust, C. (2010) Analysis of the dispersion of large unconfined clouds following a massive spillage of liquid helium on the ground. International Conference on Harmonisation within Atmospheric Dispersion Modelling for Regulatory Purposes (HARMO 13), Paris, France.

2.1.7 Takeno et al. (1994)

Takeno and co-workers measured the evaporation rates of liquid hydrogen and liquid oxygen spilled on different ground surfaces contained in a vacuum-insulated cylindrical glass Dewar. The different ground surfaces investigated were i) limestone concrete, ii) dry layer of sand and iii) a layer of sand with 7% water content to imitate rainfall conditions. Two vessel sizes were used for the experiments with liquid hydrogen: 50 mm diameter and 600 mm length and 100 mm diameter for 200 mm length. The volume of liquid used were 500, 1000 and 1500 cm^3. The vessel dimensions and the quantity of fuel were varied to investigate the thermal influence of the vessel wall and the gravitational influence of the liquid. They found out that in both wet and dry sand, the liquid hydrogen would not soak into it due respectively to the water and the air freezing creating a thin layer on top of the sand. For the concrete layer, the liquid just vaporized above it. In all cases, the variation of evaporation rate with time was proportional to $t^{-1/2}$, except in the starting phase of vaporization.

Reference :

Takeno, K., Ichinose, T., Hyodo, Y. and Nakamura, H. (1994) Evaporation rates of liquid hydrogen and liquid oxygen spilled onto the ground. Journal of Loss and Prevention in the Process Industries, Vol. 7(5), pp. 425-431.

2.1.8 HSL experiments (2010)

In 2010, unignited liquid hydrogen release experiments were performed by HSL in Buxton, UK. The tests were conducted on a 32 m diameter concrete pad.

Figure 10 : Pictures of the HSL setup.

Four tests were conducted :

- tests 6 and 10 consisted of a vertically downward release 100 mm above the ground,
- test 7 was a horizontal release 860 mm above the ground,

- test 5 was a horizontal release onto the ground.

LH_2 was released in the experiments at a constant rate of 60 L/min for all tests, but the release velocity was not measured. The diameter of the orifice was 26.3 mm and the storage pressure was measured to be 2 bara (absolute pressure). The release point was after a 20 m vacuum line of 1" diameter and there was no pre-cooling of the line with LN_2. The LH_2 tank headspace is first depressurized to 1 bara producing a subcooled LH_2 in the storage. Then with the pressure buildup external loop, the tank is pressurized to 2 bara. The source term conditions are difficult to estimate due to these two opposite phenomena (flash in line and subcooling).

The wind speed was measured at the edge of the pad at a height of 2.5 m. The temperature was also measured but no information was available for atmospheric stability and surface roughness length.

Numerous thermocouples were used allowing to assess the pool size, the hydrogen distribution (assuming adiabatic mixing) and the concrete temperature during the release.

Reference :

Hooker, P., Willoughby, D. B., Hall, J. and Royle, M. (2012) Experimental releases of liquid hydrogen. Hazards XXIII.

2.1.9 Common weak points of these studies

The main weak point of these experiments is the lack of data for the initial release conditions. temperature and pressure at the orifice, possible flashing in piping, LH_2 thermodynamic conditions (saturated or subcooled) are unknown. Moreover, the discharge rate is sometimes unclear.

The second weak point is the lack of instrumentation (concentration, temperature, velocity, fluctuations, …) used to understand the physic, limited to few spatial locations. Hence, valuable comparison with CFD modelling is quite difficult.

2.2 Pressurized releases

2.2.1 High momentum releases

Source term

Cryogenic hydrogen choked release experiments were performed by Simoneau and Hendricks from NASA (1979) in an elliptical converging-diverging nozzle with 2.934 mm throat diameter. Examined hydrogen stagnation conditions were in the range $0.82 < T_0/T_{cr} < 0.98$ and $0.995 < P_0/P_{cr} < 4.54$ corresponding to the sub-cooled liquid regime.

These choked flow experiments were successfully simulated by Travis et al. (2012) using a Homogeneous Non-Equilibrium flash Model (HNEM), that accounts for liquid

superheat through a constant, prescribed "non-equilibrium" parameter. The exact value of this parameter used in the simulations was not reported. The computed results appeared to be consistently greater than the measured mass fluxes, but within 10% of the latter.
The same experiments were successfully simulated by Venetsanos and Giannissi (2017) using the Homogeneous Equilibrium Model (HEM) for flash calculations. Predicted critical mass fluxes were found generally overestimated, but within 10% of the experimentally measured values.
In both works above, the NIST EoS for H_2 (see Leachman et al., 2009) was used in the critical flow simulations.
An excellent review work on computational modelling of flash boiling flows was recently presented by Liao and Lucas (2017). HEM model generally underestimates critical mass fluxes compared to models that account for liquid metastable conditions (e.g. superheat).

References :

Simoneau, R., Hendricks, R. (1979) Two-phase choked flow of cryogenic fluids in converging-diverging nozzles. NASA Tech. Rep. Pap. 1484.

Travis, J., Koch, D., Breitung, W. (2012) A homogeneous non-equilibrium two-phase critical flow model. International Journal of Hydrogen Energy Vol. 37(22):17373-9.

Venetsanos, A.G. and Giannissi, S.G. (2017) Release and dispersion modeling of cryogenic under-expanded hydrogen jets. International Journal of Hydrogen Energy Vol. 42(11): 7672-7682.

Leachman, J.W., Jacobsen, R.T., Penoncello, S.G., Lemmon, E.W. (2009) Fundamental equations of state for parahydrogen, normal hydrogen, and orthohydrogen. Journal of Physical and Chemical Reference Data Vol. 38(3):721-48.

Liao, Y., Lucas, D. (2017) Computational modelling of flash boiling flows: A literature survey. International Journal of Heat and Mass Transfer 111: 246–265.

Dispersion experiments

The experiments described by Breitung *et al.* (2009) consisted of release and ignition of horizontal liquid hydrogen jets at temperature of 35 to 65 K and pressures from 7 to 35 bars at Karlsruhe Institute of Technology (KIT) in the framework of the ICEFUEL project. They performed a total of 37 experiments, divided in three campaigns, of liquid hydrogen releases through a small orifice of 0.5 or 1 mm (from 2 to 8 g/s). They studied the distribution process (temperature and concentration) in cryogenic unignited jets. The hydrogen concentrations were measured for different nozzle diameters and reservoir conditions (pressure and temperature).

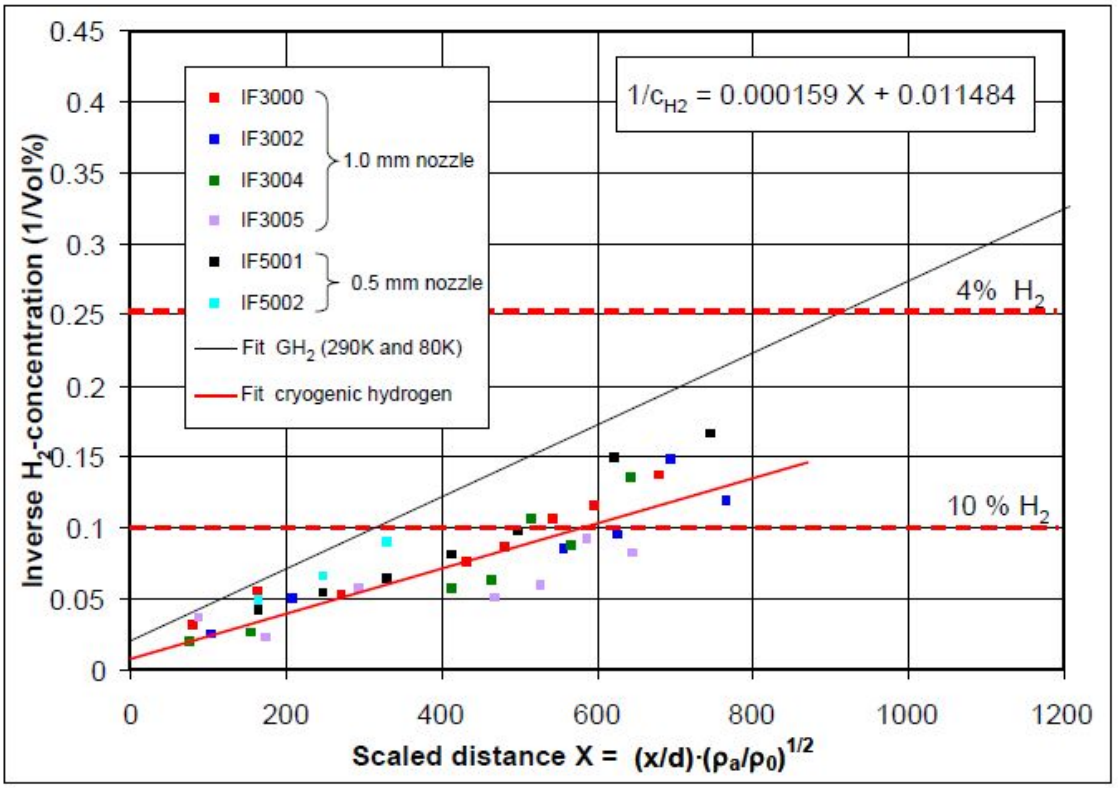

Figure 11 : Summary of measured axial hydrogen concentrations in case of cryogenic and gaseous hydrogen release.

It is interesting to notice that the distance to 4% is larger for cryogenic release than for cold or ambient gaseous release.

Recently, Hecht and Panda (2018) performed vertical cryogenic hydrogen releases (1 & 1.25 mm diameter) at low pressure (2 to 5 bars) and low nozzle temperature (50 to 61K), using spontaneous Raman scattering. They studied the distribution of concentration (average centerline and half-width of mass fraction, radial profiles) and temperature decay. They compared the radial mass fraction and temperature at selected distances with 2 fits based on their releases and one based on the available literature (room temperature jets). They also used the mole fraction and temperature fields for comparison with the ColdPlume model which gave good predictions. It should be interesting to compare these results with the correlation proposed by KIT.

T_{noz} [K]	P_{noz} [bar_{abs}]	d [mm]
58	2	1
56	3	1
53	4	1
50	5	1
61	2	1.25
51	2.5	1.25
51	3	1.25
55	3.5	1.25
54	4	1.25

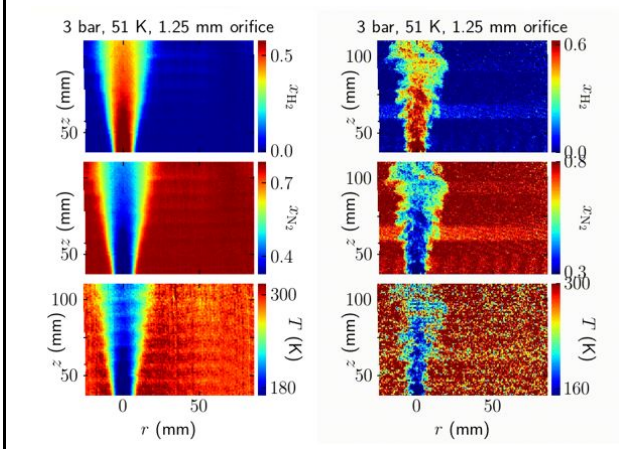

Figure 12 : Conditions and examples of the SNL cryogenic releases.

Lately, Kobayashi *et al.* (2018) completed a serie of horizontal leaks of cryogenic hydrogen pressurized up to 90 MPa at temperature of 50, 200 and 300K. They performed 17 experiments, described in Figure 13, of supercritical hydrogen releases through pinhole nozzles of 0.2, 0.4, 0.7 and 1 mm diameters. They studied the concentration distribution and leakage flow rates. The hydrogen leakage flow rate was measured for the different outlet diameters (0.2, 0.4, 0.7 and 1 mm) and supply temperatures (50, 200 and 300 K). The hydrogen concentration distribution was obtained by injecting high-pressure hydrogen from the 0.2 mm pinhole for 10min.

	D [mm]	Supply condition[a]	P_0 [MPa]	T_0 [K]	m [g/s]
1	0.4	C	22.1	76.2	3.63
2	0.4	C	43.5	64.9	6.04
3	0.4	C	78.4	65.9	8.87
4	0.4	C	21.1	62.1	3.78
5	0.4	C	41.8	54.9	6.07
6	0.4	C	82.2	61.5	9.20
7	0.7	C	21.0	68.2	11.19
8	0.7	C	38.0	61.8	17.07
9	0.7	C	61.3	62.2	23.42
10	0.2	H	82.1	281.5	1.19
11	0.2	C	84.7	64.4	2.33
12	0.2	M	83.7	170.0	1.77
13	0.2	C	41.5	59.5	1.49
14	0.2	C	84.7	65.9	2.32
15	0.2	C	84.0	66.3	2.31
16	0.2	C	84.0	61.0	2.33
17	0.2	C	90.0	68.3	2.39

[a] C: Low-temperature conditions (50 K), H: Ambient-temperature condition (300 K), M: Intermediate temperature condition (200 K).

Figure 13: Experimental conditions for the hydrogen releases.

They concluded that when the supply temperature decreases, the leakage flow rate increases and the hydrogen concentration increases. They also offered a new empirical formula to determine the 1% concentration distance based on the leakage flow rate.

References :

Breitung, W., Stern, G., Veser, A., Friedrich, A., Kuznetsov, M., Fast, G., Oechsler, B., Kotchourko, N., Travis, J.R., Xiao, J., Schwall, M., Rottenecker, M. (2009) Experimental and theoretical investigations of sonic hydrogen discharge and jet flames from small breaks - ICEFUEL final report.

Hecht, E., Panda, P. (2018) Mixing and warming of cryogenic hydrogen releases. International Journal of Hydrogen Energy, July 2018.

Kobayashi, H. et al. (2018) Experiment of cryo-compressed (90 MPa) hydrogen leakage diffusion. International Journal of Hydrogen Energy.

2.2.2 Low momentum releases

Winters and Houf (2011) studied steady-state leaks with large amounts of pressure drop along the leak path such that hydrogen enters the atmosphere at near atmospheric pressure (i.e. very low Mach number).

They developed a three-stage buoyant turbulent entrainment model to predict the properties (trajectory, H_2% and temperature) of a jet emanating from the leak depending if the leak occurs from the saturated vapor space or saturated liquid space.

In the first stage of the entrainment model, ambient temperature air (295 K) mixes with the leaking hydrogen (20–30 K) over a short distance creating an ideal gas mixture at low temperature (~65 K). During this process, states of hydrogen and air are determined from equilibrium thermodynamics using models developed by NIST.

In the second stage of the model the radial distribution of H_2% and velocity in the jet develop into a Gaussian profile characteristic of free jets.

The third and by far the longest stage is the part of the jet trajectory where the flow is fully established.

While trajectories for ambient temperature jets depend solely on the leak densimetric Froude number, results from the present study show that cold jet trajectories depend on the Froude number and the initial jet density ratio.

The figure 14 gives a simple outcome of the work performed.

Table 2 – Dilution distance to 4% hydrogen mole fraction concentration for 3 types of multi-phase hydrogen leaks.

Pipe ID (mm)	Leak diameter[d] (mm)	Distance[e] (m)
Saturated vapor leak[a]		
6.35 mm (1/4 inch)	1.100	4.431
12.7 mm (1/2 inch)	2.200	8.861
19.05 mm (3/4 inch)	3.299	13.29
25.4 mm (1 inch)	4.399	17.71
31.75 mm (1.25 inch)	5.499	22.13
38.10 mm (1.5 inch)	6.599	26.55
44.45 mm (1.75 inch)	7.699	30.96
50.80 mm (2 inch)	8.799	35.36
Saturated liquid leak[b]		
6.35 mm (1/4 inch)	1.100	5.659
12.7 mm (1/2 inch)	2.200	11.26
19. 05 mm (3/4 inch)	3.299	16.75
25.4 mm (1 inch)	4.399	22.11
31.75 mm (1.25 inch)	5.499	27.31
38.10 mm (1.5 inch)	6.599	32.37
44.45 mm (1.75 inch)	7.699	37.29
50.80 mm (2 inch)	8.799	42.06
Subcooled liquid leak[c]		
6.35 mm (1/4 inch)	1.100	9.611
12.7 mm (1/2 inch)	2.200	15.9
19.05 mm (3/4 inch)	3.299	21.94
25.4 mm (1 inch)	4.399	27.64
31.75 mm (1.25 inch)	5.499	33.09
38.10 mm (1.5 inch)	6.599	38.34
44.45 mm (1.75 inch)	7.699	43.46
50.80 mm (2 inch)	8.799	48.4

a Leak from saturated vapor space at 1.03 MPa (150 PSIG).
b Leak from saturated liquid space at 1.03 MPa (150 PSIG).
c Leak from subcooled liquid at 1.03 MPa (150 PSIG) and density of saturated liquid (65 kg/m^3) at 0.207 MPa (30 PSIG).
d Diameter based on 3% of pipe flow area.
e Distance to location where hydrogen concentration is 4% by volume.

Figure 14 : Distance to 4% for various low momentum releases.

Obviously, results show that flammability envelopes for cold hydrogen jets are generally larger than those of ambient temperature jets.

For the same diameters and pressure, the largest distance to 4%H_2 is for the subcooled liquid leaks (possibly even worst if there is rainout) followed by saturated liquid leaks and saturated vapor leak (the shortest distance to 4%).

References :

Winters, W.S. and Houf, W.G. (2011) Simulation of small-scale releases from liquid hydrogen storage systems. International Journal of Hydrogen Energy, Vol. 36(6), pp. 3913-3921.

2.3 Remaining knowledge gaps on release and mixing phenomena

Based on the previous analysis of the literature, the remaining knowledge gaps are :

- Characteristics of flashing, multiphase, multicomponent releases in well defined thermodynamic conditions (subcooled, saturated) including rainout and pool formation, droplet granulometry and volumetric concentration;
- Mass and heat transfer including phase transition (pool evaporation, condensing and freezing of contaminants) in LH_2 releases;
- Free cryogenic jet structure, morphology and behaviour in realistic conditions, in particular accounting for wall attachment and/or surface impingement;
- Phenomena influencing the mixing of LH_2 releases (from a heavy cold gas to a buoyant gas) in a cross-wind and possible interaction with safety barriers as water spray.

3 Ignition phenomena

There are various hazards associated with explosive atmospheres which can lead to its ignition and explosion.
The European standard EN1127:1:2011 details a variety of ignition sources hazardous within an explosive atmosphere. These include:
- Hot surfaces
- Flames and hot gases (including hot particles),
- Mechanically generated sparks,
- Electrical apparatus,
- Stray electrical currents and cathodic corrosion protection,
- electrostatic discharge (spark, brush or corona),
- Lightning,
- Radio Frequency/ electromagnetic waves from 10^4 Hz to $3x10^{11}$ Hz,
- Electromagnetic waves from $3x10^{11}$ Hz to $3x10^{16}$ Hz,
- Ionizing radiation,
- Ultrasonics,
- Adiabatic compression and shock waves,
- Exothermic reactions.

Astbury and Hawksworth (2007) and Merilo *et al.* (2012) suggest that there are 5 potential mechanisms of ignition for pressurized hydrogen releases : reverse Joule-Thomson effect, electrostatic ignition, diffusion ignition, sudden adiabatic compression and hot surface ignition. However, Astbury and Hawksworth (2007) concluded that the reverse Joule-Thomson effect, sudden adiabatic compression and hot surface ignitions were unlikely to occur in practice hence

the majority of ignitions occurring are due to diffusion ignition, with electrostatic ignition also being a viable mechanism when ignition by diffusion cannot provide an explanation. There are also reported occurrences of condensed phase ignition as discussed later.

3.1 Flammability limits at low temperatures

The data on flammability limits at low temperatures fit very well to the corresponding data for ambient and elevated temperatures. Figure 15 includes experimental and theoretical data on flammability and self-ignition (auto-ignitions) limits in a wide range of temperatures and concentrations for hydrogen–air mixtures at ambient pressure. The domain below the self-ignition limit and between the lower and upper flammability limits corresponds to flammable mixtures area ignited by extra ignition sources (spark, glow plug, hot surface).
Summarizing all the experiments in the range -150 – 400°C, Kuznetsov *et al.* (2013) recommend to use the following linear interpolation for the lower flammability limit (LFL) :

$$C_{LFL}[vol.\%] = 4.64 - 0.0067 \cdot t[^{o}C]$$

where C_{LFL} is the unknown lower flammability limit for a given temperature t [ºC].The lower flammability limit of hydrogen at the ambient temperature t = 0 ºC is C_{LFL} = 4.64 vol. %H_2.

Summarizing all the experimental in the range -60 – 400°C, Kuznetsov *et al.* recommend to use the following linear interpolation for the upper flammability limit (UFL) :

$$C_{UFL}[vol.\%] = 73.8 + 0.033 \cdot t[^{o}C]$$

where C_{UFL} is the unknown upper flammability limit for a given temperature t [ºC]. The upper flammability limit of hydrogen at the ambient temperature t = 0 ºC is C_{UFL} = 73.8 vol. %H_2 .

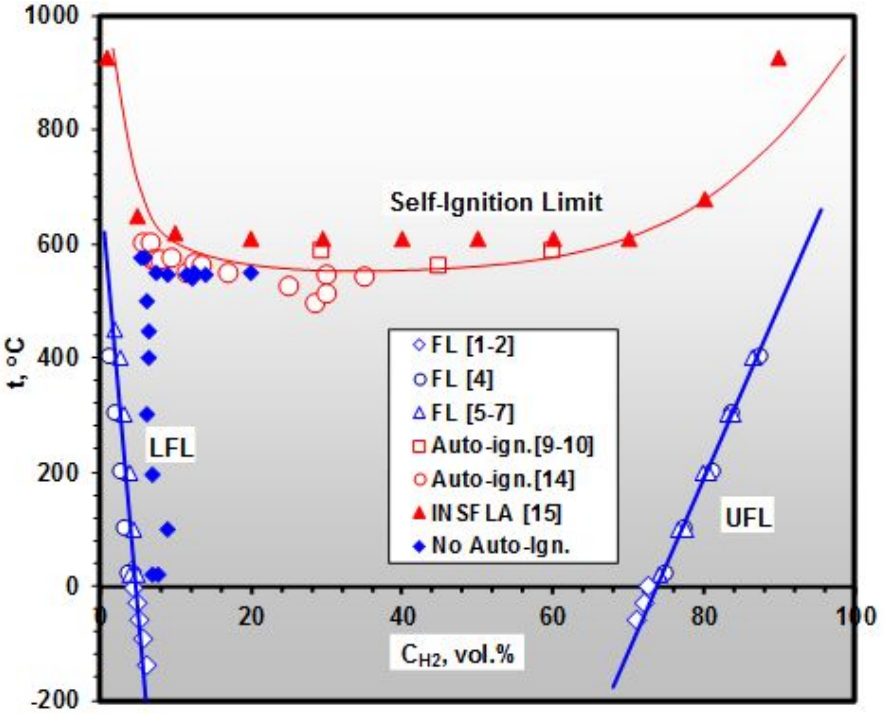

Figure 15 : Flammability limits at atmospheric pressure as a function of initial temperature.

The influence of low temperature on flammability limits for horizontal and downward flame propagation is unknown.

References :

Astbury, G.R. and Hawksworth, S.J. (2007) Spontaneous ignition of hydrogen leaks: a review of postulated mechanisms. International Journal of Hydrogen Energy, vol. 32, pp. 2178-2185.

Kuznetsov M., Czerniak M., Grune J., Jordan T., Effect of temperature on laminar flame velocity for hydrogen-air mixtures at reduced pressures. Proc. of the 5th International Conference on Hydrogen Safety, ICHS 2013 September 9-11, 2013 - Brussels – Belgium, paper 231, p. 1-12.

Merilo E.G., Groethe M.A., Adamo R.C., Shefer R.W., Houf W.G. and Dedrick D.E.(2012) Self-ignition of hydrogen releases through electrostatic discharge induced by entrained particulates," International Journal of Hydrogen Energy, vol. 37, no. 22, pp. 17561-17570.

3.2 Minimum Ignition energy (MIE)

Semi-empirical correlations obtained from 300 to 200K by Martín-Valdepeñas and Jiménez (2003) for lean and rich hydrogen-air compositions is extrapolated for lower temperatures. Obviously, the MIE increases with initial temperature decreasing within the cryogenic

domain.

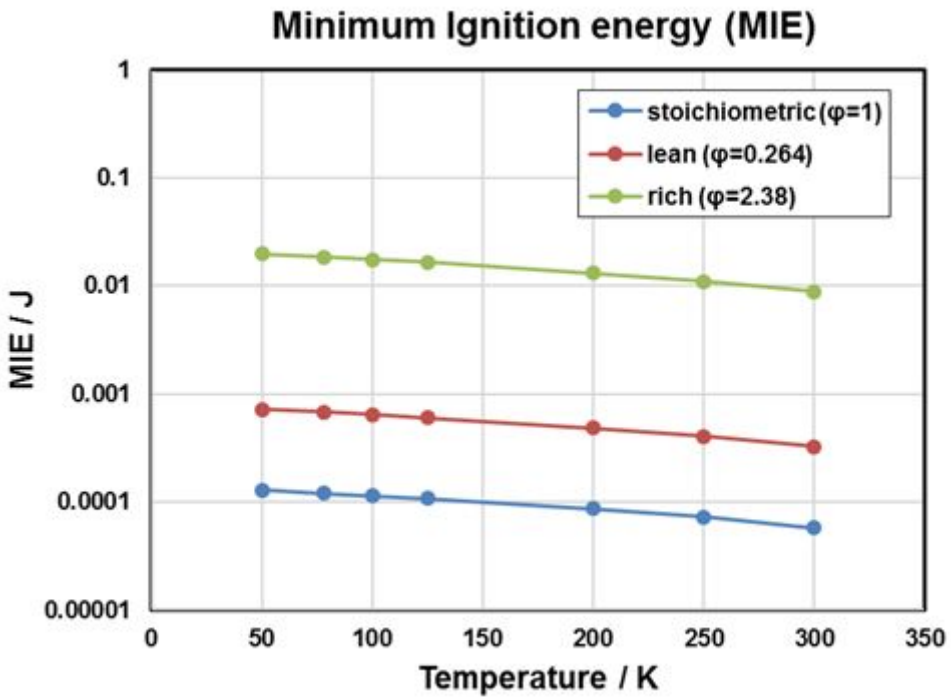

Figure 16 : Minimum Ignition Energy at atmospheric pressure as a function of the initial temperature for 3 equivalence ratios (extrapolations below 200 K).

The figure 16 also shows a strong MIE increase for lean and rich hydrogen – air mixtures in comparison with stoichiometric one. The difference is of the order of magnitude of one or two for lean and rich respectively.

Reference :

Martín-Valdepeñas J.M., Jiménez M.A. (2003) Exploring MIE as a Safety Indicator Parameter in Practical Applications. Universidad Politécnica De Madrid Escuela Técnica Superior De Ingenieros Industriales, Cátedra De Tecnología Nuclear, EU-Fifth Framework Programme (1998-2003), Contract EVG1-CT-2001-00042, EXPRO - Experimental and Numerical Study of Reactive Flows with Relevance to Industrial Safety for Explosion Protection, CTN-09/03, November 2003.

3.3 Ignition by corona discharges

Ignition by corona discharge generally occurs in areas of high field strength and can develop around sharp points with a radius of curvature less than 3 to 5mm (Merilo *et al.* (2012)).

Hooker *et al.* (2011) report ignition by corona discharges occurring in 26%H_2 and 33%H_2 in air at ambient temperature. The corona currents appear to vary with the square of the applied potential. The experimental program considered positive and negative potentials

being applied to the wire. The application of negative potentials to the wire did not lead to any ignitions.
Grabarczyk (2013) conducted experiments on ignition of hydrogen and carbon disulphide mixtures with atmospheric air by positive corona discharge. He concluded that ignition by low energetic positive corona discharge could occur in a hydrogen-air mixture.

Ignition of ambient temperature gaseous hydrogen by corona discharge could potentially occur at the outlet of a high vent stack in situations where the potential is tens of kV above the surrounding atmosphere (Hooker *et al*. (2011)). Such incendive corona discharges appear to be unlikely in horizontal releases of gaseous H_2 close to ground level, although this may be more likely for releases of LH_2 due to greater electric fields caused by charged clouds.
It is possible that an earthed vent pipe would be at a positive potential relative to the condensation cloud during venting of LH_2, if the cloud was charged negatively. If the electric field is strong enough due to a large negatively charged cloud then it is possible for a corona discharge to happen and, possibly, ignition to occur. This is important as ignition may occur even if equipment is earthed. However, it is not known whether ignition by corona discharges can happen at low temperatures.

References :

Merilo E.G., Groethe M.A., Adamo R.C., Shefer R.W., Houf W.G. and Dedrick D.E.(2012) Self-ignition of hydrogen releases through electrostatic discharge induced by entrained particulates," International Journal of Hydrogen Energy, vol. 37, no. 22, pp. 17561-17570.

Hooker P., Royle M., Gummer J., Willoughby D. and Udensi J. (2011) Self Ignition of Hydrogen by various mechanisms. Health and Safety Laboratory, Symposium series No. 156, Hazards XXII.

Grabarczyk Z.J. (2013) Laboratory ignition of hydrogen and carbon disulphide in the atmospheric air by positive corona discharge. Journal of Electrostatics 71: 1041-1045.

3.4 Electrostatic ignition

Low temperature hydrogen releases induce condensation of humidity and also oxygen. It is suspected that these solid particles and/or liquid droplets may facilitate the ignition by electrostatic charging.

It should be noticed that for industrial unignited (voluntary) ventings, ignition is often reported when the weather is snowy. Electrostatic charging of snow particles is invoked as a reason. These ventings are generally at low velocities i.e. less than 30 m/s at the tip.

Similar events have also been observed for ventings of cryogenic LH_2, see [https://www.nasa.gov/pdf/513855main_ASK_41s_explosive.pdf] .

These phenomena will depend strongly on the release characteristics, mass flow rate and speed, temperature and pressures, on the mixing processes with the ambient atmosphere and the general conditions of the latter, i.e. temperature, humidity and electrostatic background field imposed by general weather conditions. Because of the complexity of such multiphase releases of cryogenic hydrogen, it is necessary to understand the effects separately when trying to improve the knowledge of the coupled effects.

In general, we distinguished between the processes which generate additional electrical charges, denominated **electrostatic charging**, and the actual **electrostatic ignition**.

An experiment performed by Merilo (2012) focuses on using charged particles to induce spark discharges from insulated conductors and corona discharges. The experiment successfully ignited the H_2 jet (at 20°C) 12 times showing that electrostatic discharge of entrained particulate is a possible self-ignition mechanism for hydrogen releases.

As electrostatic charging seems to be primarily related to cryogenic hydrogen releases, a few models for this phenomena presented by Kelly (1989) are listed and associated with their relevance for LH_2 risk evaluation:

Corona charging

Corona charging is obtained by ion bombardment. A gas is charged when passing between high voltage electrodes. As the particles passed between the electrodes, they are charged by the present ions. Such a charge involves a high potential difference and is unlikely to happen accidently.

Induction charging

Induction charging occurs when a conductive particle is placed in an electric field, induced for example by a charged surface. If the particle touches the surface, it becomes permanently charged. Once charged, the particle is repelled form the surface carrying the same polarity charge.

Tribocharging

Tribocharging, or frictional charging, is the appearance of opposite charges during a contact. It can occur during solid-solid, solid-liquid or liquid-liquid contact. The two bodies become oppositely charged and an electric field is created between them. Non-conductors are locally charged on their surface. Because of the small contact area, repeated contact is needed to build a significant charge.

Even if this effect has been known for centuries and has been the source of considerable losses in the pneumatic conveying of powder materials, exact mechanisms involved are still not fully understood. There are many suggestions on charge transfer and a large number of parameters seems to influence the process, especially for non-conductors.

Charge separation during aerodynamic breakup

Droplets entrained in high velocity flow are subject to strong aerodynamic forces. These forces can cause the droplet to breakup. The breakup of liquid droplets is a well know process. It occurs mostly through the bag mechanism. The drop becomes flat, then a pouch inflates in the middle and bursts into a multitude of micro droplets.

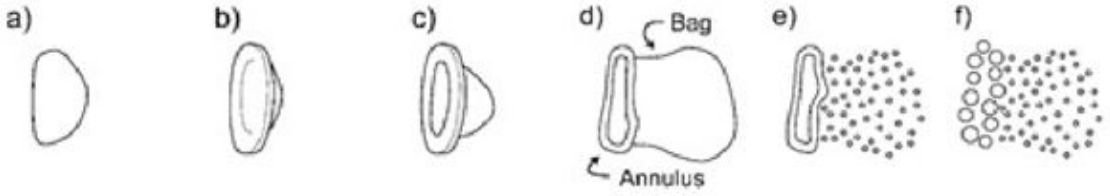

Figure 17 : Aerodynamic breakup.

Aerodynamic breakup of droplets leads to charge separation. This phenomenon is linked to the double layer at the surface of liquids. When surrounded by a gas the outer layer of a droplets is dominated by negative charges. During the breakup, the thin bag is also dominated by negative charges, so the droplets are created. The larger droplets created from the annular ring are positively charged.

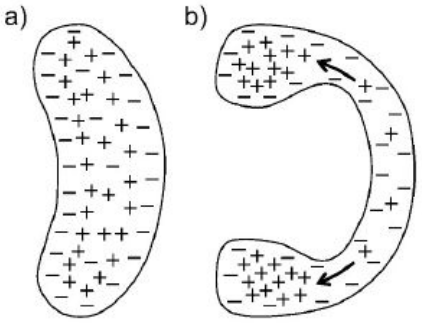

Figure 18 : Charge separation in bursting droplet.

Free falling droplets

A study has investigated the hypothesis that droplets of various liquids can build up a charge while falling through the air from a sufficient height (Lüttgens, 2015). The experiments are performed along a 5m drop with several ring shaped electrodes.

The measurements showed that there was no charge evolution during the fall and concluded that friction with air during a free fall cannot on its own and under normal conditions charge a droplet.

High pressure water - Dispersing charges

Spraying of water, as with high pressure cleaners, has been identified to be the cause of ignition of flammable atmospheres leading to severe accidents. The spraying of liquid under high pressure produces a cloud of charged droplets (Post, 1989). The study investigated under which conditions a high space charge density can occur and might induce ignitable gas discharges.

Field strength measurements were made on a horizontal open jet, along the horizontal axis with measuring heads placed 50cm under the center of the jet. The jet was released through a 1.2 mm diameter nozzle under various pressures.

A significant electric field was present around the jet. The change in sign of the electric field for large distances is induced by small suspended droplets, charged, for most, negatively through aerodynamic breakup.

References :

Merilo E.G., Groethe M.A., Adamo R.C., Shefer R.W., Houf W.G. and Dedrick D.E.(2012) Self-ignition of hydrogen releases through electrostatic discharge induced by entrained particulates," International Journal of Hydrogen Energy, vol. 37, no. 22, pp. 17561-17570.

Kelly, E.G. (1989) The theory of electrostatic separations: A review part ii. particle charging, Minerals Engineering, vol. 2, no. 2, pp. 193-205..

Lüttgens, S., Lüttgens, G., Thulin, A., Paillat, T. and Touchard, G. (2015) Electrostatic charge measurements of droplets of various liquids falling over a large distance," Chemical Engineering Technology, vol. 38, no. 7, pp. 1261-1268.

Post, L. (1989) The avoidance of ignition hazards due to electrostatic charges occurring during the spraying of liquids under high pressure," Journal of Electrostatics, vol. 23, pp. 99-109.

3.5 Ignition of LH_2/Condensed O_2 phase

The solubility of LO_2 in LH_2 is very limited. It means that for O_2 concentrations higher than few ppm, O_2 becomes a solid in form of small crystals dispersed in LH_2. This maximum O_2 concentration is the solubility and after this critical concentration, O_2 could obviously be added indefinitely in LH_2 (as salt in brine).

The mixture LH_2/solid oxygen is well known as a high explosive.

Rico (1970) studied theoretically and experimentally in his PhD this reactive mixture.

Theoretically, he obtained the following properties for a stoichiometric mixture :

- Detonation pressure P_{CJ} ~ 31 000 bar,
- Isochore combustion pressure P_{CV} = 16 000 bar,
- Detonation temperature T_{CJ} ~ 5730 K,
- Detonation velocity D ~ 5130 m/s.

The calculated detonation velocity increases to 5130 m/s at an equivalence ratio of Φ=1 ($1H_2$+ ½ O_2) to 9330 m/s at Φ=5 ($5H_2$+ 1/2 O_2 i.e. 91%H_2) (similar to TNT). On the other side, the detonation pressure reduces from 31 000 to 27 000 bars at Φ = 1 and 5 respectively.

Experimentally, Rico generated this reactive mixture by injecting gaseous oxygen in LH_2 in long dewars. To avoid that O_2 crystals fall in the lower part of the dewar, a small flow rate of helium was injected to obtain homogeneity.

Figure 19 : Experimental setup for studying LH_2/Solid O_2 detonation.

The mixture detonation initiated by detonators (lead azide) was demonstrated by the measurement of the aerial overpressure and by visual inspection of the mechanical effects. Quantitative results were obtained by measurement of the detonation velocity with optic fibers. Detonation velocities of 5000 m/s at Φ = 3.5 and 8250 m/s at Φ = 4.5 were measured in good agreement with the theoretical study.

Similar conclusions (but less instrumented experiments) were obtained by NASA (1969) on the basis of aerial overpressure measurements.

In Arthur D. Little experiments, explosion of LH_2/solid oxygen mixtures are also reported but the composition of the mixture is unclear.

Litchfield E.L. and Perlee H.E. (1964) performed experimental research on the shock sensitivity of LH_2 and solid O_2 by deliberately creating mixtures with O_2 and N_2 and igniting them by firing them with high velocity projectiles. The results were produced by mixing O_2 and N_2 in the gas phase and condensing to solids by cooling the mixture using the vapors from boiling liquid hydrogen. The same amount of oxygen was used for each test whilst the amount of liquid hydrogen was varied to ensure that the condensate was covered with hydrogen at the point of firing of the projectile.

A velocity of 506 m/s (1660 ft/s) had a 50% probability of initiation of the undiluted liquid hydrogen-solid oxygen mixture, i.e. the basic explosive system with no diluent has a 50% probability of detonation.

Litchfield produced a table in the report providing information in relation to the dilution of the liquid hydrogen, solid oxygen and solid nitrogen detailing the lowest velocity producing initiation, the highest velocity not producing initiation and their ratios to the 50% velocity of the undiluted mixture. This is reproduced in the figure 17.

The failure velocity is the highest velocity at which initiation did not occur whereas the initiation velocity is the lowest velocity at which initiation resulted. He also indicated that the shock strength (i.e. pressure) is proportional to the projectile velocity. Therefore, the velocity ratio is then the approximate ratio of the pressure produced in the test and the pressure required for 50% probability of initiation.

At 47% dilution the shock strength required for initiation is doubled. For a 78% nitrogen dilution of the oxygen would increase the require shock initiation by a factor of at least three.

Percent N_2 in condensate	Initiation		Failure	
	Velocity, ft/sec	Velocity ratio	Velocity, ft/sec	Velocity ratio
0	1,660	1.00	1,660	1.00
23	2,280	1.39	1,950	1.20
47	3,580	2.16	3,250	1.96
78	insufficient velocity available		4,880	2.94

Figure 20 : Litchfield analysis of the initiation velocity of Liquid Hydrogen, Solid Oxygen and Solid Nitrogen.

It has to be mentioned that in HSL experiments, after the end of the LH_2 release (of 4.5 minutes), a secondary explosion of a solid formed occurred one time out of 10 experiments. This solid explosive could be a lean LH_2/solid oxygen mixture (too much oxidant compared to H_2). Moreover in air, nitrogen also becomes solid leading to a

dilution of the reactive heterogeneous mixture. Based on windows damages in a nearby storage building, the estimate of the TNT equivalent is less than 4 kg meaning approximately 100 g of hydrogen.

References :

Rico H.Y. (1970) Etudes théorique et expérimentale de la détonation des mélanges d'hydrogène liquide et d'oxygène solide à 20 K. Thèse de doctorat de l'Université de Paris.

Litchfield E.L. and Perlee H.E. (1964) Fire and explosion Hazards of Flight Vehicle combustibles. April 1 to June 30, 1964, Quarterly Progress Report No. 2, Explosives Research Centre, US Department of the Interior.

Litchfield E.L.and Perlee H.E. (1964) Fire and Explosion Hazards of Flight Vehicle Combustibles. Quarterly Progress Report No. 1, January 2 to March 31, 1964.

3.6 Remaining knowledge gaps

Based on this literature survey, the knowledge gaps to be filled are :

- Influence of low temperature on horizontal and downward flammability. This point is important to consider a credible size of the flammable cloud in case of delayed ignition;
- Minimum ignition energy and ignition energies of cold H_2 / air mixtures;
- Electrostatic charging and ignition.

The formation and explosion properties of mixtures of LH_2 with solid oxygen is well documented. As a consequence, this topic is not considered of a priority in the experimental program.

References :

Wierzba, I., Harris, K., Karim, G.A. (1992) Effect of low temperature on the rich flammability limits in air of hydrogen and some fuel mixtures containing hydrogen. International Journal of Hydrogen Energy Vol. 17, Issue 2, February 1992, Pages 149-152.

Karim G.A., Wierzba I., Boon S. (1984) The lean flammability limits in air of methane, hydrogen and carbon monoxide at low temperatures. Cryogenics, 24(6), pp.305–308.

Gasse A. (1992) Experimentelle Bestimmung und Simulation von Explosiongrenzen, untersucht an wasserstoffhaltigen Brenngasgemischen. Dissertation Universitat-Gesamthochschule Paderborn, Reihe Verfahrenstechnik, Shaker, Aachen.

Kumar R.K. (1985) Flammability limits of hydrogen-oxygen-diluent mixtures. AECL-8890. Journal of Fire Sciences, 3:235-262.

Hustad J.E., Sonju O.K. (1988) Experimental studies of lower flammability limits of gases and mixtures of gases at elevated temperatures. Combustion and Flame 71:283.

DeSoete .G.G. (1975) Overall kinetics of nitric oxide formation in flames. La Revista dei Combustibili. 29:166.

Omar M.H.,Dokoupil Z. (1962) Solubility of nitrogen and oxygen in liquid hydrogen at temperatures between 27 and 33°K. Physica, Vol. 28, issue 5.

High R.W. (1969) Some liquid oxygen / liquid hydrogen explosive effects in controlled failure mode tests. NASA report.

Zabetakis M.G. (1965) Flammability characteristics of combustible gases and vapors, Bureau of Mines Bulletin 627, p. 121.

Astbury, G. R., and Hawksworth, S.J. (2005) Spontaneous ignition of hydrogen leaks: A review of postulated mechanisms. Proceedings of International Conference on Hydrogen Safety.

4 Combustion phenomena

4.1 Cryogenic Jet-fire

Panda and Hecht (2016) studied ignited cryogenic hydrogen free releases. They showed that the correlation established for gaseous releases could be used for cryogenic releases.

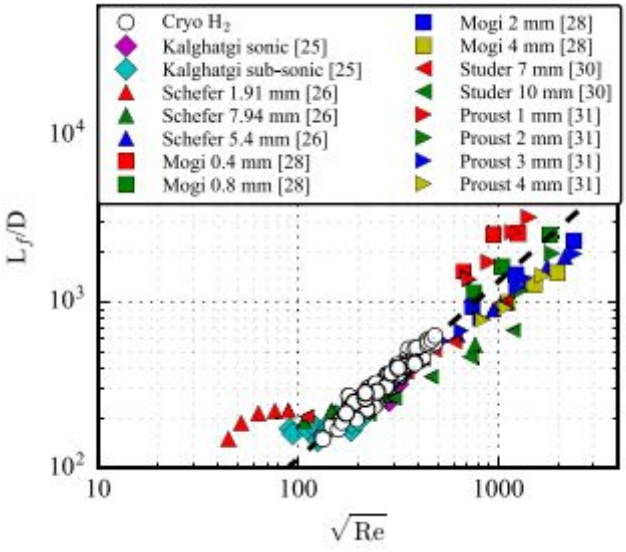

Figure 21 : Flame length correlation.

In the figure 21, the equation of the proposed correlation is :

$$\frac{L_f}{D} = 0.86\sqrt{Re}$$

Compared to the expression proposed by Molkov and Saffers (L_f # $(m.D)^{1/2}$) for atmospheric temperature hydrogen releases, this expression allows to take into consideration the variations in viscosity induced by the cold releases.

The Reynolds number is calculated on the throat density, viscosity, choked flow velocity, and diameter.
The figure 22 presents the radiative fraction for various flame conditions.

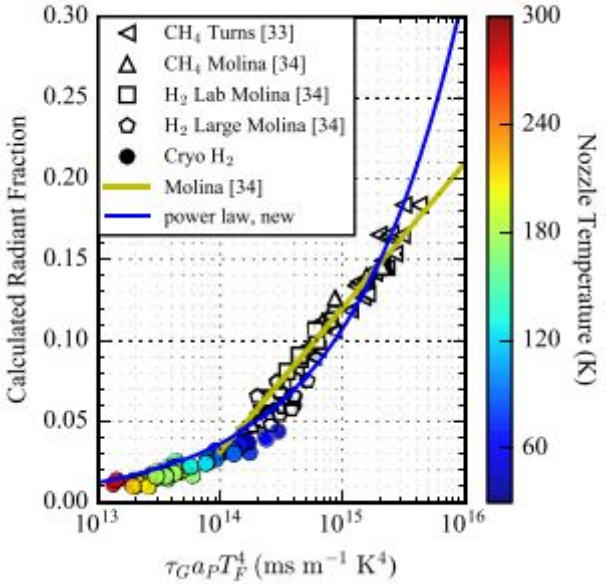

Figure 22 : Radiative fraction for various flames.

On the figure 22, the power law equation is :

$$\chi_r = 9.45 \times 10^{-9}\left[a_p \tau_G T_f^4\right]^{0.47}.$$

with $a_p = 0.23$.

It should be noticed that it is not clear if T_f is calculated accounting the initial low temperature conditions.

In the equation, $\boldsymbol{\tau}_G$ is the residence time in the jet fire expressed as :

$$\tau_G = \frac{\rho_f W_j^2 L_f f_s}{3\rho_o D^2 V_j}.$$

In the framework of the ICEFUEL project, Breitung *et al.* also performed experiments with cryogenic releases (from 7 to 35 bars and from 34 to 65 K respectively - diameter of 1 and 0.5 mm). Radiative levels of the flames were measured at a fixed radial location. The axial sensor locations were 1200 and 1300 mm, respectively, and the radial distance from the jet axis was 750 mm. They suggest a radiative fraction X_{rad} of 6% for cold (80K) and cryogenic flames which is higher than X_{rad} = 3% measured by the same authors in ambient conditions.

Cryogenic jet fires were investigated in a numerical study conducted by Cirrone *et al.* (2017). The aim of the study was to develop and validate a computational fluid dynamics (CFD) model to predict flame length and radiative heat flux at different locations from the flame. The simulation results were compared against the experimental tests conducted at Sandia National Laboratories on cryogenic hydrogen fires (Panda and Hecht, 2016).
The Reynolds-Averaged Navier-Stokes (RANS) CFD model was based on the realizable κ-ε turbulence model, as it demonstrated the best performance in reproduction of experimental flame length and radiative heat flux. The Eddy Dissipation Concept (EDC) was employed for hydrogen combustion in air with inclusion of 18 elementary reactions and 9 species. Radiative heat transfer was taken into account through the Discrete Ordinates (DO) model. Ulster's notional nozzle theory was used to model the release sources, demonstrating a good agreement with the measured mass flow rates. A relatively good agreement is obtained for flame length and radiative heat flux.

References :

Panda P.P. and Hecht E.S. (2017) Ignition and flame characteristics of cryogenic hydrogen releases. International Journal of Hydrogen Energy, Vol. 42, Issue 1, 5 January 2017, Pages 775-785.

Friedrich A., Breitung W., Sterna G., Veser A., Kuznetsov M., Fast G., Oechslerb B., Kotchourko N., Jordan T., Travis J.R., Xiao J., Schwall M., Rottenecker M. (2012) Ignition and heat radiation of cryogenic hydrogen jets. International Journal of Hydrogen Energy Vol. 37, Issue 22, November 2012, Pages 17589-17598.

Schefer R.W., Houf W.G. , Bourne B., Colton J. (2006) Spatial and radiative properties of an open-flame hydrogen plume. International Journal of Hydrogen Energy, Vol. 31, Pages 1332-1340.

Turns S.R. and Myhr F.H. (1991) Oxides of nitrogen emissions from turbulent jet flames: Part I—Fuel effects and flame radiation. Combustion and Flame 87 , 319-335.

Cirrone D., Makarov D. and Molkov V,(2017) Thermal radiation from cryogenic hydrogen jet fires. International Conference on Hydrogen Safety, Hamburg, Germany, Sept. 11-13.

4.2 Pool fire

According to the work of Hottel (1958), Zabetakis (1967) and Babrauskas (1983) for hydrocarbons, equations for predicting the regression rate of a pool fire are proposed in the literature. The figure 23 presents the regression rate for LH_2, LNG and gasoline.

Fluid	Density [kg/m^3]	ΔH_v [kJ/kg]	ΔH_c [MJ/kg]	k β $^{(1)}$ [m^{-1}]	T_f $^{(1)}$ [K]	$\dot{m}_\infty$ $^{(2)}$ [mm/min]	$\dot{v}_\infty$ $^{(3)}$ [mm/min]
LH_2	71	446	120	6.1	1600	142.2	20.5
LNG	422	510	61	1.1	1500	11.1	9.1
LPG	544	428	46	1.4		10.9	8.2
Gasoline	737	330	44	2.1	1450	4.5	11.3

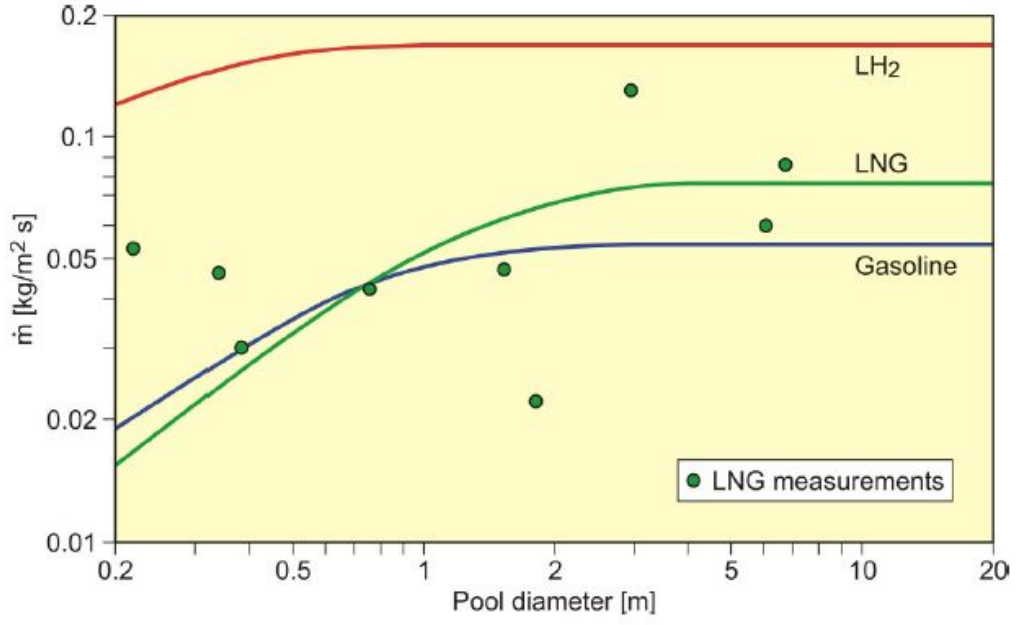

Figure 23 : Regression rate as a function of pool diameter.

It has to be noticed that the figures are only extrapolations of a model developed for gasoline. A verification for LH_2 would be interesting.

It has to be clear that the surface burning rate can be easily calculated from regression rate using a LH_2 density of 70.9 kg/m^3.

In the IDEALHY Deliverable 3.11 "Qualitative Risk Assessment of Hydrogen Liquefaction, Storage and Transportation" written by Hankinson and Lowesmith from Loughborough University (2013), the mass burning rate considered for LH_2 was 0.15 $kg.m^{-2}.s^{-1}$ for a large pool (which is in good agreement with the figure).

For flame height calculations, there is no specific correlations in the litterature. As a consequence, classical correlations are widely used (Iqbal, 2004, for instance).

$$H_f = 0.235 * P^{0.67} - 1.02*D$$

with P the flame power (kW) and D the pool diameter (m).

Concerning the radiative effects, there is very little open litterature. Hankinson and Lowesmith (2013) assumed a fraction of heat radiated of 0.15. However, a value of 0.25 was cited by Zabetakis and Burgess (1961) for LH_2 pool fires.

References :

Zabetakis M.G. and Burgess D.S. (1961) Research in Hazards Associated with the production and Handling of Liquid Hydrogen US Bureau of Mines Report, RI5707.

Hankinson G. and Lowesmith B.J. (2013) IDEALHY Deliverable 3.11 "Qualitative Risk Assessment of Hydrogen Liquefaction, Storage and Transportation".

Babrauskas V. (1983) Estimating large pool fire burning rates. Fire Technology, November 1983, Volume 19, Issue 4, pp 251–261.

Hottel H.C. (1959) Certain Laws Governing Diffusive Burning of Liquids. Fire Research Abstr. Rev. 1. p.41.

Zabetakis M.G. (1967) Safety with Cryogenic Fluids. Pp 98-113 - Plant and Test Site Safety.

Iqbal N., Salley M.H., Weerakkody S. and NRC Project Manager (2004) Fire Dynamics Tools (FDTs): quantitative fire hazard analysis methods for the U.S. nuclear regulatory commission fire protection inspection program. NUREG-1805, Division of System Safety and Analysis, Office of Nuclear Reactor Regulation, U.S. Nuclear Regulatory Commission, Washington DC, December 2004.

4.3 Deflagration

AICC Pressure (Adiabatic IsoChoric Combustion)

The pressure generated by an adiabatic isochoric combustion PAICC were calculated using the EXPLPRESS freeware (SAFEKINEX). This explosion pressure is higher when the initial temperature decreases. For instance, for H_2/air stoichiometric mixture at atmospheric pressure, PAICC equals to 8 bar at 300 K increases to 12 and 23.5 bar respectively for 200 and 100 K.

The STANJAN code base on NASA thermodynamic database is also able to calculate the PAICC pressure, even to 78K in an assumption of ideal gas (figure 24). It gives the same value of 23.5 bar at 100K and 30.1 bar at 78K corresponding to liquid nitrogen boiling temperature at atmospheric pressure.

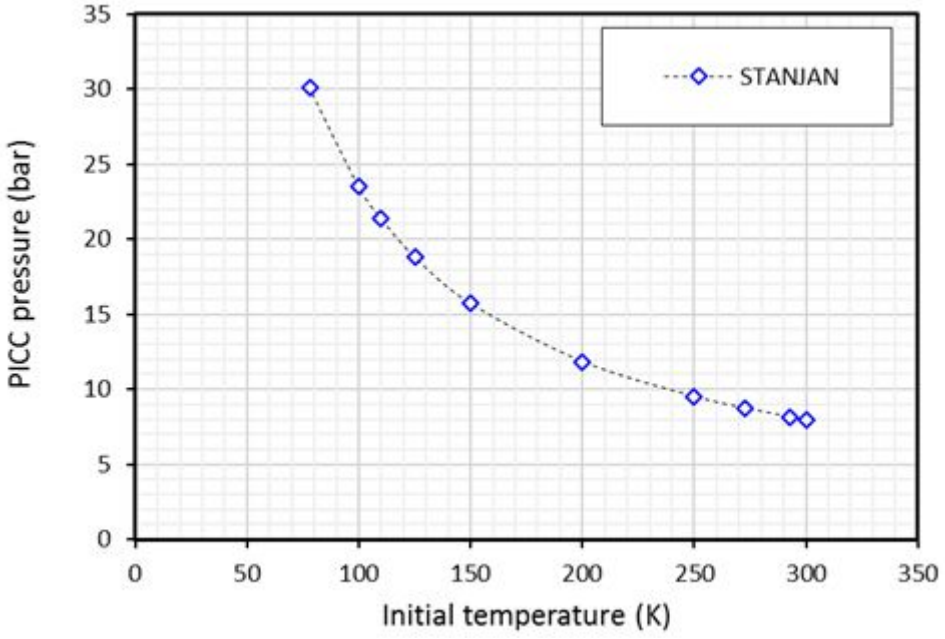

Figure 24 : PAICC as a function of initial temperature for stoechiometric H_2/air mixture at atmospheric pressure.

Expansion ratio (σ)

The expansion ratio (σ) is the ratio of the density of the fresh gases (unburnt before ignition) by the density of the burnt gases (at flame temperature). This is an important parameter for combustion processes and flame acceleration because it represents the piston effect of the flame. This may result in formation of turbulent flow and advancing shock waves in front of the flame. The visible flame velocity S_f and flow velocity U_f ahead of the flame are proportional to the expansion ratio (σ) and to the laminar flame velocity (S_L).

$$S_f = \sigma \cdot S_L$$

$$U_f = (\sigma - 1) \cdot S_L$$

Thermodynamic calculations with STANJAN code demonstrated very weak influence of initial temperature on adiabatic combustion temperature. For instance, for a change in initial temperature from 300 K to 78 K (four times), the adiabatic combustion temperature varies less than 5% from 2383 K to 2263 K respectively.

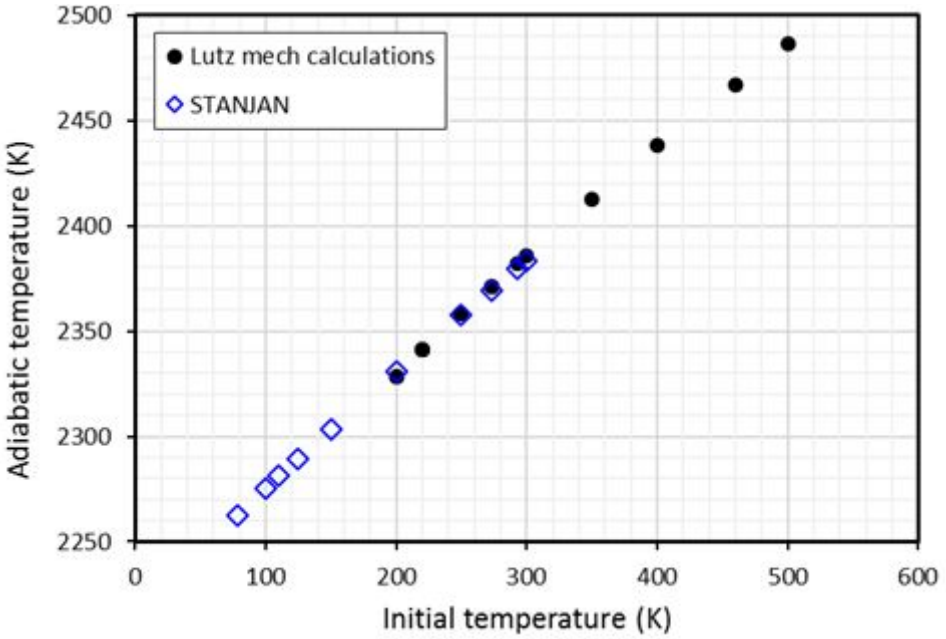

Figure 25 : Adiabatic flame temperature as a function of initial temperature for an atmospheric stoechiometric H_2/air mixture.

This means that the expansion ratio may also increase roughly by four times assuming a real gas equation of state. As shown in Bavoil PhD thesis (1997), the expansion ratio increases for low temperature. For a stoichiometric mixture at atmospheric pressure the expansion ratio is equal to 7 at 300K and increases to 20 at 100 K. The same value of expansion ratio σ = 19.53 for stoichiometric H_2-air mixture at 1 bar and 100K was calculated by using the STANJAN code. At 78K the code gives a value σ = 24.88.

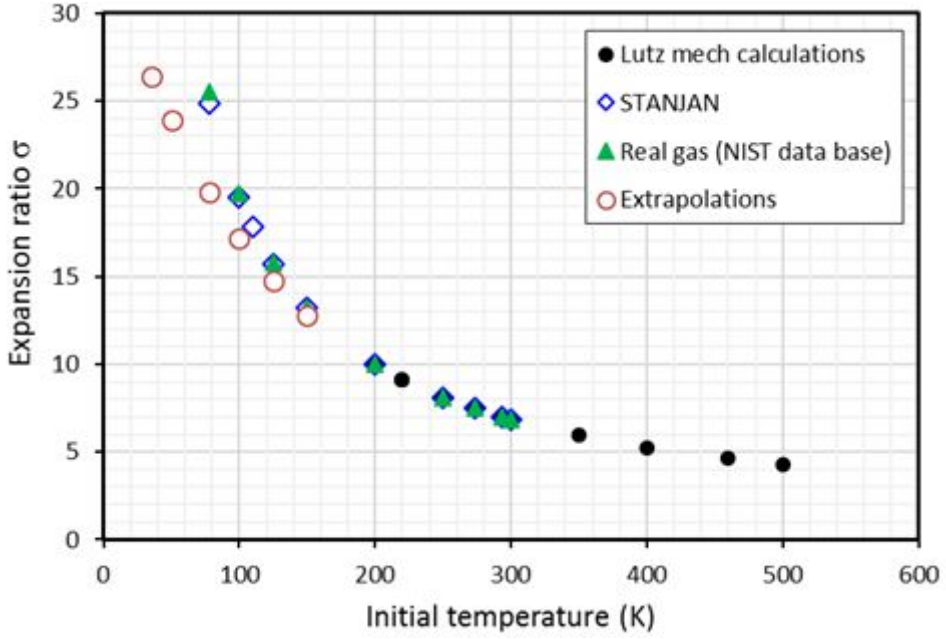

Figure 26 : Expansion ratio as a function of initial temperature for an atmospheric stoechiometric H_2/air mixture.

Taking into account the real gas state (according to the NIST database), at lower initial temperatures, the expansion ratio will be not so much changing in comparison with ideal gas state: σ = 19.73 (T = 100K); σ = 25.53 (T = 78K).

Laminar flame speed

Using a spherical bomb and the pressure trends, Bavoil (1997) studied the influence of cold initial temperature on the laminar flame speed of H_2/air mixtures from 100 to 300K for different equivalence ratio (Rich on the figure 27). For different equivalence ratio (Richesse in french) he proposed values of alpha to calculate the laminar flame speed in low temperature conditions.

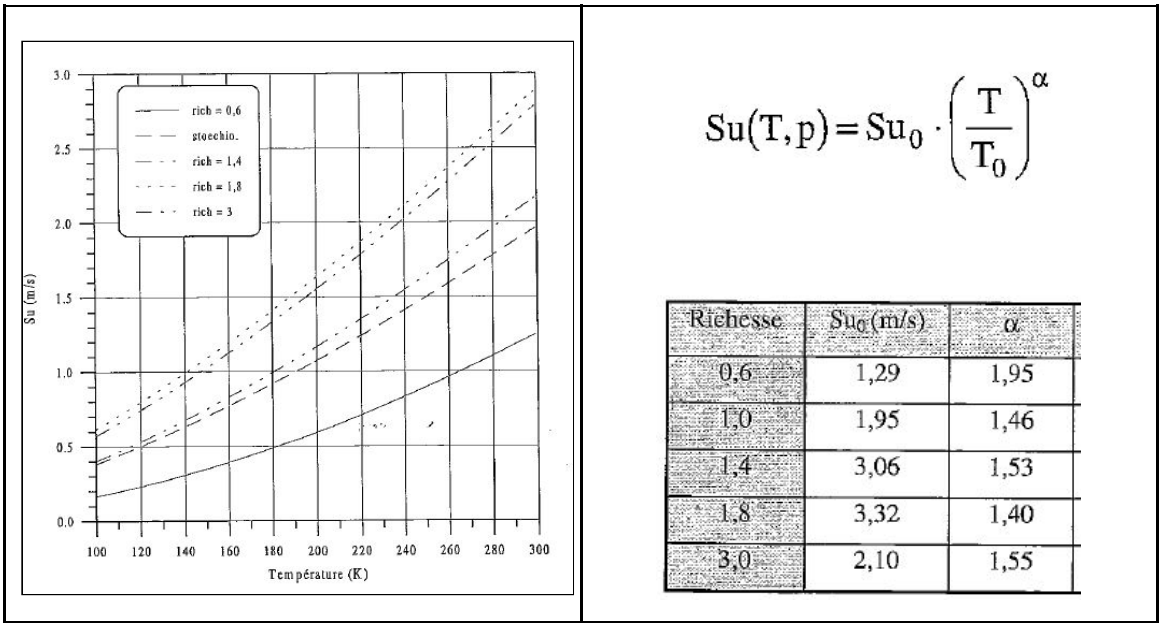

$$Su(T,p) = Su_0 \cdot \left(\frac{T}{T_0}\right)^{\alpha}$$

Richesse	Su_0 (m/s)	α
0,6	1,29	1,95
1,0	1,95	1,46
1,4	3,06	1,53
1,8	3,32	1,40
3,0	2,10	1,55

Figure 27 : Laminar flame velocities measured by Bavoil.

The laminar flame velocity at different initial conditions can also be directly calculated using a Cantera code with detailed chemistry (Lutz scheme in this particular case). The figure below demonstrates the dependence of laminar flame velocity with low temperatures. The capability of the code was limited by 200K. Then, the dependence was extrapolated to 78K. The figure shows an over-prediction of theoretical calculations compared to experimental data: S_L = 0.71 m/s against 0.4 m/s (100K). Extrapolation to 78K gives the value S_L = 0.59 m/s.

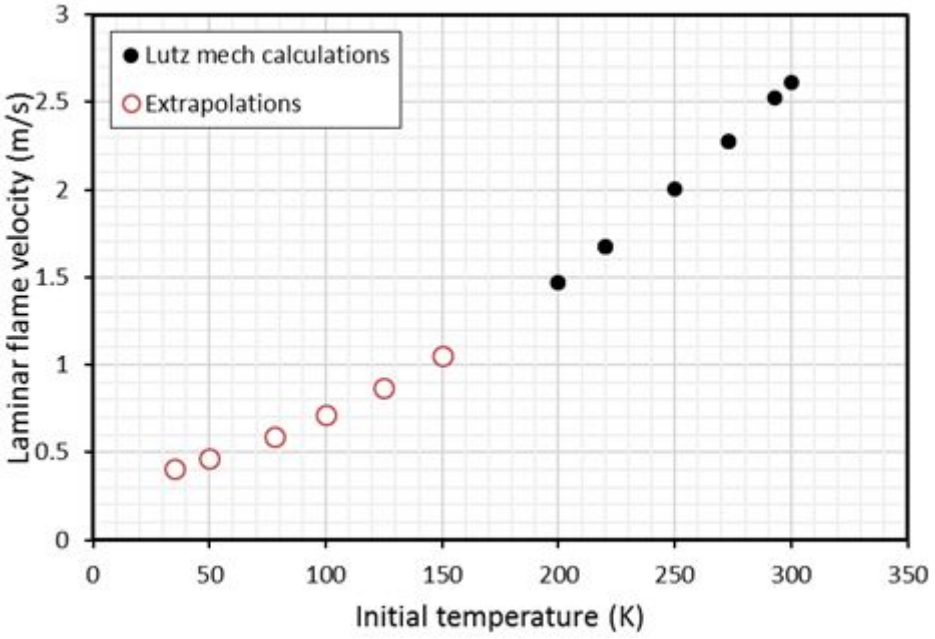

Figure 28 : Calculated Laminar flame velocities as a function of the initial temperature for an atmospheric stoechiometric H_2-air mixture.

As we mentioned above, the product of laminar flame speed times expansion ratio as a visual flame velocity is an integral characteristic of flame acceleration potential. As another figure shows, reduced chemical reactivity at cryogenic temperatures will be compensated by higher density and in turns by higher expansion ratio of the gas at low temperatures. In general, visible flame velocity 11.7 m/s is only two times lower than that 25.7 m/s at ambient conditions.

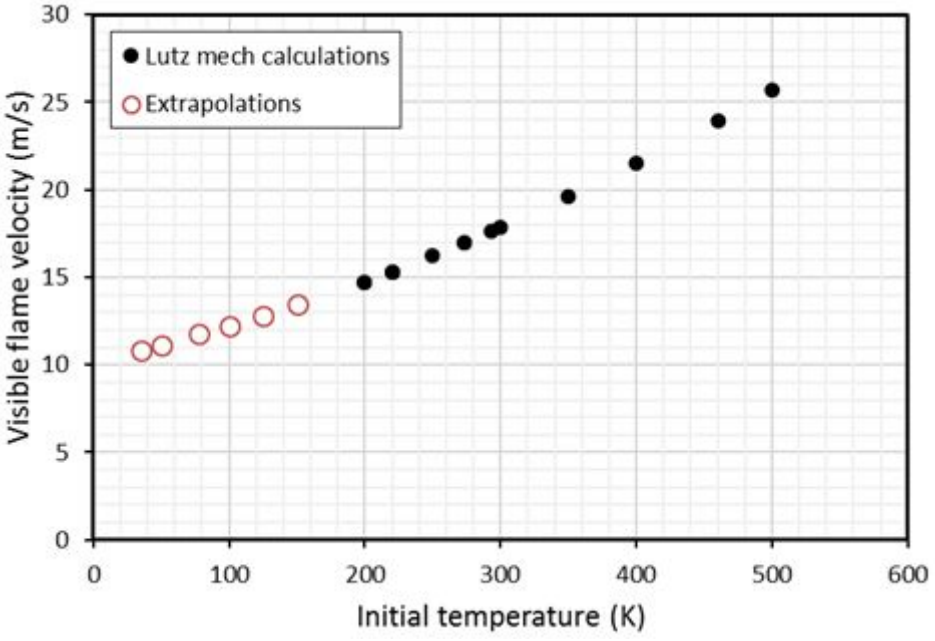

Figure 29 : Calculated visible flame velocity as a function of the initial temperature for an atmospheric stoechiometric H_2-air mixture.

Flame propagation regimes at cryogenic temperatures

Within the flammability limits, three typical combustion regimes can be distinguished for gaseous mixtures. These include slow subsonic deflagrations ($v < c_r$ - flame velocity v is less than the speed of sound in reactants c_r), fast supersonic flame ($c_r < v < c_p$ - flame velocity was less than the speed of sound in products c_p, but more than the speed of sound in reactants), and detonation ($v = D_{CJ}$). All possible regimes are shown schematically in Figure 30 below for hydrogen-air mixtures at initial pressure 1 bar.

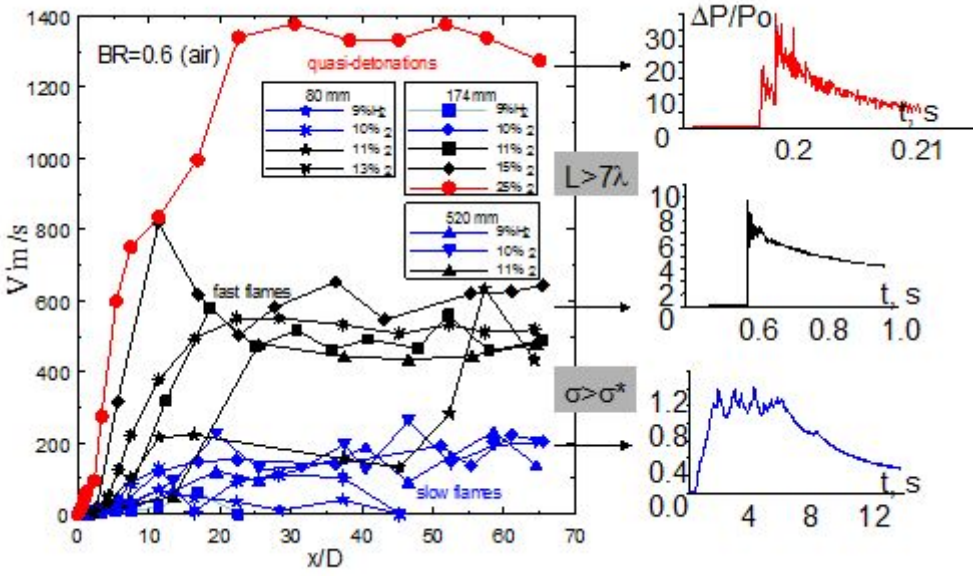

Figure 30 : Combustion regimes for different hydrogen-air mixtures (P = 1 bar, T = 293 K): right pictures correspond to pressure signals for different regimes.

As it was suggested by Dorofeev and co-authors, expansion rate σ^* and 7λ criteria can be considered as potentials of strong flame acceleration and detonation onset correspondingly. Mixtures with expansion rate σ above the critical value σ^* can effectively accelerate and then detonate, if the detonation criteria $L > 7\lambda$ is satisfied (L is the characteristic size of combustible domain, λ is the detonation cell size). The mixtures with $\sigma < \sigma^*$ can not accelerate effectively and only subsonic combustion regime may occur. Characteristic pressure loads from combustion process is a function of combustion regime and can change from 1-2 bar for slow combustion, to 6-8 bar for sonic flames and 20-40 bar for detonation, for an initial pressure of 1 bar.

Critical sigma

The critical expansion ratio σ^* is a function of dimensionless integral scale (L_T - turbulent length scale, d -laminar flame thickness) and Zeldovich number b ($b = E_a(T_b-T_u)/T_b^2$). The critical expansion ratio σ^* decreases with initial temperature T_u increase and overall energy activation E_a decrease.

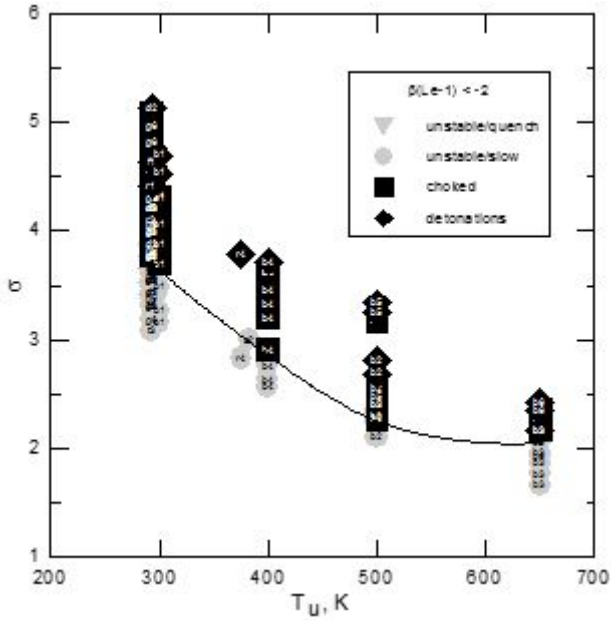

Figure 31 : Resulting combustion regime as a function of expansion ratio σ and initial temperature T_u for H_2 – air mixtures.

(black points – fast ; gray points - slow combustion regimes)

Dependence of critical expansion ratio vs. Zeldovich number looks almost linear. This means that the overall activation energy E_a shouldn't be independent of the initial temperature. Otherwise the dependence of σ^* with temperature Tu would be linear.

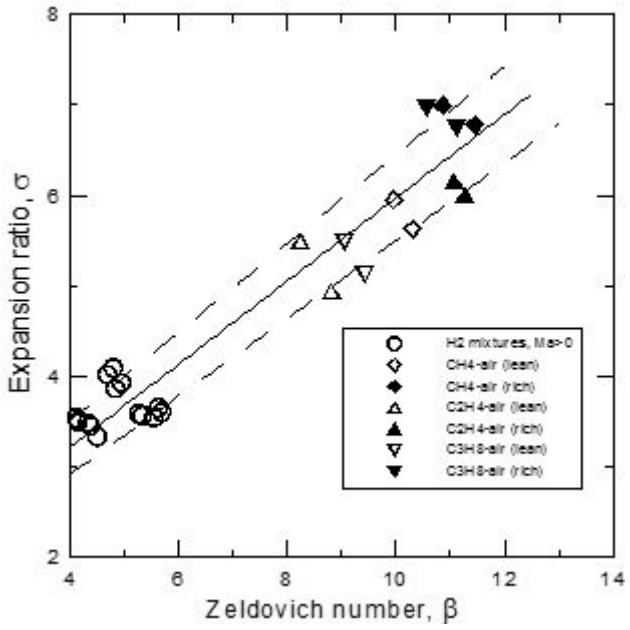

Figure 32 : Critical mixture expansion ratios for possible development of fast flames in obstructed channels vs. a Zeldovich number.

Figure 33 shows critical expansion ratio σ^* for cryogenic temperatures. This figure also gives the threshold H_2% for an effective flame acceleration to flame speed higher than speed of sound. It follows from the data that the lower hydrogen concentration for flame acceleration to speed of sound reduces from 11 to 9%H_2 with temperature decrease from 300K to 78K.

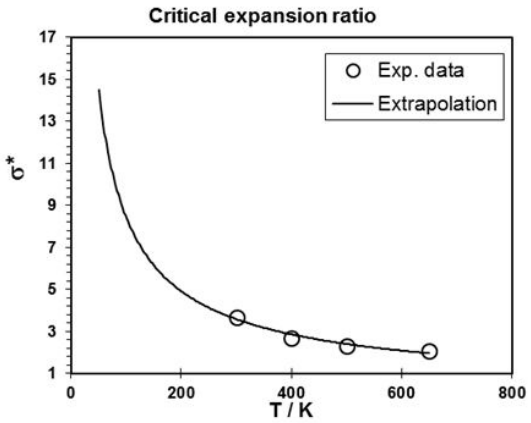

T, K	C_{H2}, %mol	σ*
300	11	3.75
200	10.34	4.92
150	10.09	6.14
100	9.58	8.49
78	9.13	10.67
50	8.60	13.89

Figure 33 : Critical mixture expansion ratios versus initial temperature : extrapolation to low temperature (solid line).

Detonation and Deflagration to Detonation Transition (DDT)

The detonation may only occur if the flame is able to reach the speed of sound ($\sigma > \sigma^*$). The only critical condition $L > 7\lambda$ should then be satisfied. This means that the characteristic geometrical size of the system should exceed seven detonation cell sizes.
There is a lack of experimental data on detonation cell size at cryogenic and reduced (lower than normal) temperatures in mixtures containing H_2. One reference only is known regarding this low pressure and temperature problem. The paper of Zitoun *et al.* (1995) gives detonation cell sizes for stoichiometric H_2-O_2 mixtures at 123K and different initial pressures.

Temperature, T (K)	Pressure, p (bar)	Detonation cell width, λ (mm)
123	0.4918	1.4819
123	0.6953	0.9901
123	0.9827	0.6889

Figure 34 : Detonation cell sizes for stoichiometric H_2-O_2 mixtures at reduced temperatures.

For H_2-air mixtures, we only have experimental data on the influence of initial temperature higher than ambient temperature on detonation cell size. In general, in accordance with referred data of Tieszen *et al.* the detonation cell size is increasing with temperature decrease. These data are covering a relatively narrow range of temperatures (278-373 K) for H_2-air mixture with $\Phi = 0.5$ In general, we can extrapolate these data to lower temperatures but not far.

The best way to resolve this problem is to compute using CELL_H2 for detonation cell calculations. The code CELL_H2 is using different chemical kinetic models and multidimensional detonation cell structure assumption and is verified for a wide range of elevated pressures and temperatures and mixture compositions. It demonstrates very good capability within the range 278-373K. The biggest problem is the low temperature limitation below 200 K due to the 200 K limit of available range of thermodynamic properties.

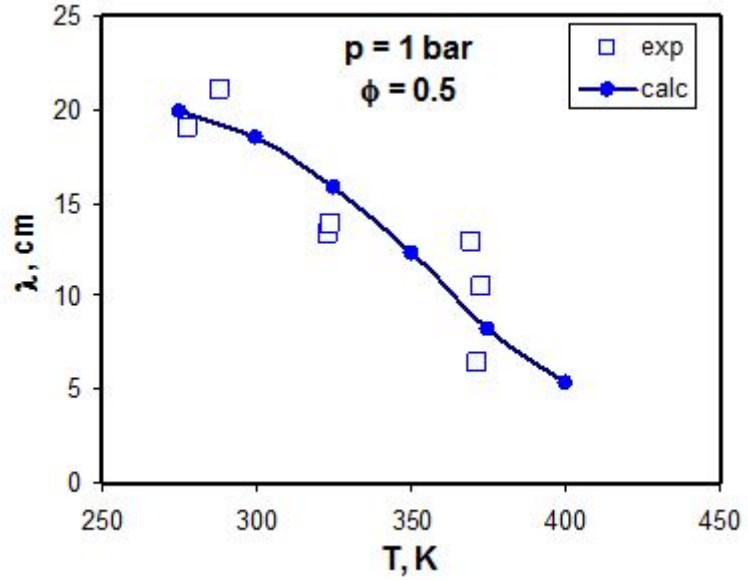

Figure 35 : Comparison of calculated and experimental detonation cell size data for H_2-air mixtures at different temperatures (p = 1 bar).

As expected, the CELL_H2 did not demonstrate a good reliability for use at cryogenic temperatures for H_2-O_2 mixtures. The code gives an under-prediction compared to experimental data, see Figure 35.

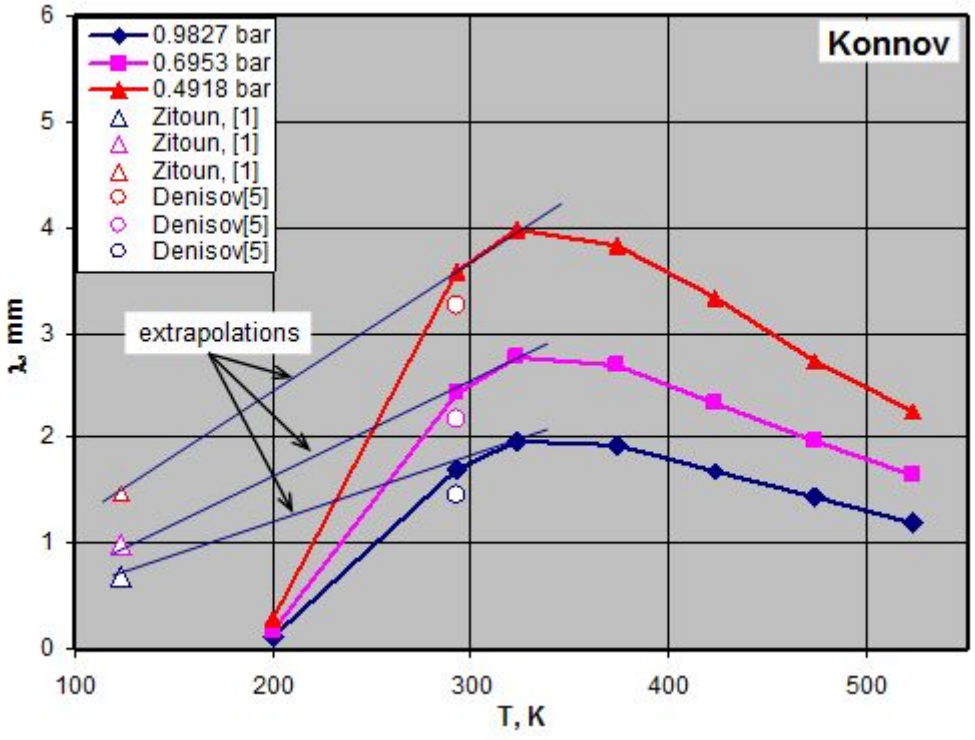

Figure 36 : Comparison of calculated and experimental detonation cell size data for H_2-O_2 mixtures at different temperatures and pressures.

The figure 36 shows an attempt to calculate the detonation cell sizes at low temperatures for hydrogen air mixtures. In general, the detonation cell size slightly increases with initial temperature decrease. Then, after it reaches its maximum, the dependence goes down but too rapid as compared with low temperature experiments. As shown in figure 36, the tangent at the maximum might be extrapolated to 100K to get more reliable data than the linear extrapolation directly from high temperature domain. Our evaluation of detonation cell sizes for 3 H_2-air compositions at different temperatures is given in the figure below.

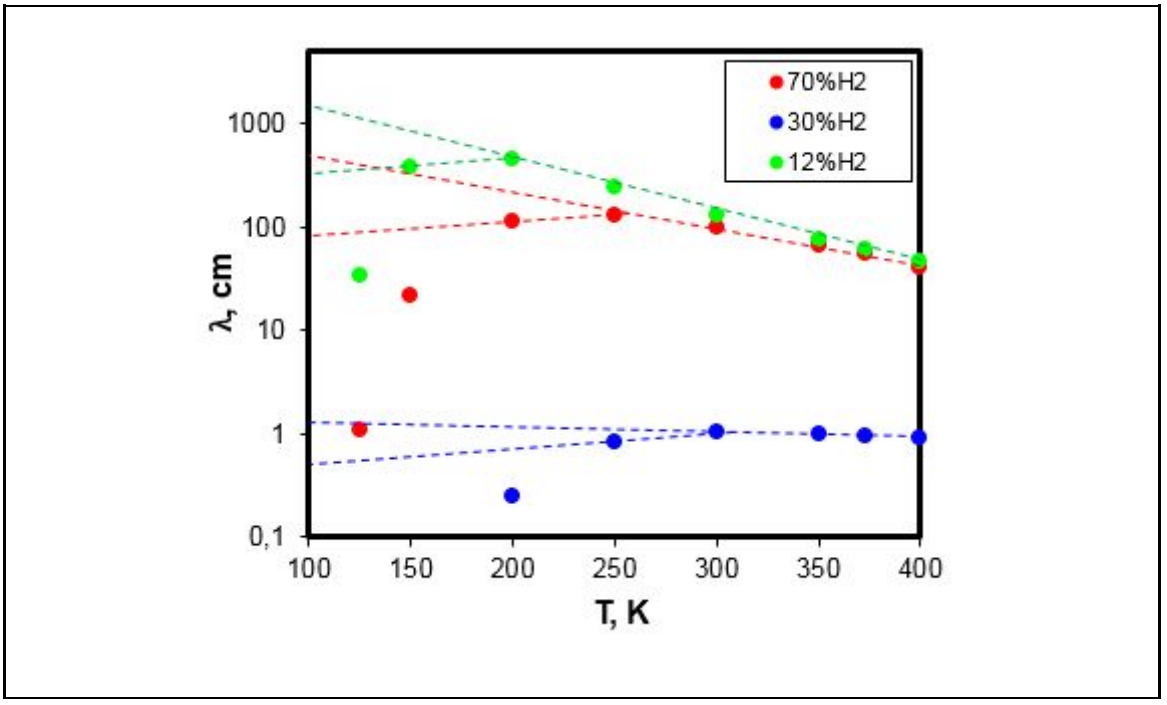

Temperature, T (K)	Detonation cell width λ, cm		
	Hydrogen concentration, %vol.		
	12	30	70
373	61	0.97	55
300	131	1.06	99
250	240	0.85	127
200	450	0.79	112
150	372	0.63	100
100	316	0.50	79

Figure 37: Detonation cell sizes for different H_2 – air mixtures at low temperatures (P = 1 bar).

Concerning DDT (in smooth or obstructed tubes), there is no published work to our knowledge.

Unconfined Unobstructed Vapour Cloud Explosion

A few studies on unconfined unobstructed VCE exist.

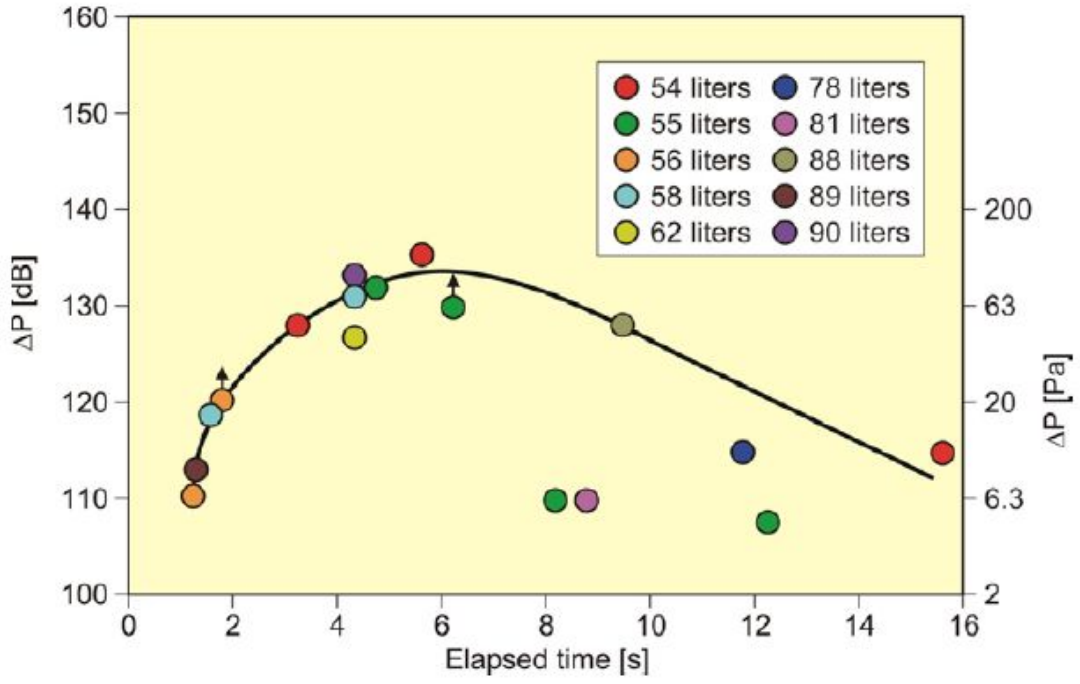

Figure 38 : Overpressure generated by unconfined uncongested vapor cloud explosion for small LH_2 spillage (<100 L) as a function of elapsed time.

In Zabetakis work (1960), for the spill and ignition tests with 54 - 90 liters of LH_2 onto a steel plate or loose gravel, the overpressures were measured (Pa end dB) at a distance of 49 m. As shown on figure 35, the blast waves produced were very small and dependant on the ignition delay time.

In Arthur D. Little work, forced ignition of small and large clouds was also investigated in order to assess the the possibility of the detonation of hydrogen-air mixtures in open space. In all the experiments, only deflagration (no detonation) were observed.

For the two small spillages, ignition was right after the spillage. For the two large spillages, the ignition was delayed. In both cases, ignitions were achieved with sparks and high explosives. It was concluded that no significant overpressure was produced and that only a flash fire with a limited radiation was produced.

In HSL experiments, 4 low momentum releases were successfully ignited (4 out of 14 tests). For these 4 tests, the overpressures generated by the explosion of the cloud were also very small. The authors stated that the safety distances are sized by the radiation effects.

Delayed ignition of pressurized LH_2 releases

In the framework of the ICEFUEL projet, Breitung *et al.* performed experiments also with cryogenic releases (from 7 to 35 bars then from 34 to 65 K respectively - diameter of 1 and 0.5 mm - less than 10 g/s). Sound levels of the flammable cloud burnout were measured. Very low overpressures (less than 120 dB(A)) were measured.

They also measured the maximum ignition and flashback axial distance. The maximum ignition distance corresponded to 7%H_2 which is in good agreement with the horizontal flammability limit usually accepted. The maximum flashback distance corresponded to 9%H_2. For ambient conditions, the flashback distance corresponded to 11%H_2 which is H_2% equivalent to a critical expansion ratio $\sigma^* = 3.75$. It is interesting to notice that this is in good agreement with the theoretical increase of the hydrogen reactivity at low temperature (see figure 33 on expansion ratio).

Unconfined Congested Vapour Cloud Explosion

In case of LH_2 spillage on an industrial site, a cold and reactive H_2/air cloud could be formed. In case of ignition, the flame could interact with the obstacles (vaporizer, pipe rack, vegetation) possibly leading to flame acceleration and even deflagration to detonation transition in the worst case scenario.

To our knowledge, there is no published experimental work on this issue.

Concerning modelling studies, a work on potential DDT in ambient vaporizer will be presented at the Mary Kay O'Connor Process Safety Center International Symposium (October 23-25, 2018 - Texas).

Computational fluid dynamic (CFD) analysis of a single vaporizer of typical construction was carried out using the FLACS code to evaluate the potential for a DDT with a vaporizer engulfed by a hydrogen-air mixture at the worst-case concentration. This analysis showed that while significant flame acceleration occurs within the vaporizer, as expected, a DDT is not predicted.
However, the analysis did indicate that a DDT may occur for two or more closely spaced vaporizers. This is relevant since multiple vaporizers are frequently present in industrial installations and are typically placed closely together to limit the required area. Spacing adjacent vaporizers further apart could preclude a DDT. However, specification of the spacing to preclude a DDT would require refined CFD analysis and/or testing, neither of which has been performed at this time.

Reference :

Thomas J.K., Geng J., Rodriquez O., Jallais S., Vyazmina E., Miller D., Lindberg B., Pawulski R. (2018) Potential for Hydrogen DDT with Ambient Vaporizers. Mary Kay O'Connor Process Safety Center International Symposium (October 23-25, 2018 - Texas).

Boiling Liquid Expanding Vapor Explosion BLEVE

A BLEVE is an event associated with the catastrophic failure of a pressure vessel containing a liquid which is stored at a temperature above its saturation temperature at atmospheric pressure. On failure, some of the liquid will flash to vapour resulting in the generation of overpressure, ignition of the released contents produces a large fireball which can determine the hazard range. This hazard is thus relevant to LH_2 which, although stored cryogenically, is also at modest pressure. Although LH_2 vessels are designed to relieve safely in the event of loss of the insulating vacuum, failure/blockage of this system could lead to a BLEVE, or fire attack could raise pressures and lead to a BLEVE with a fireball due to inadequate venting of pressure. Experimental data on BLEVEs is available for butane, propane, LNG, but no information has been identified for LH_2.

Some empirical relationships exist in the litterature to determine the diameter of a fireball D, the height the fireball achieves H, and the duration of the fireball t based on the mass of fuel involved. For LH_2 BLEVE, Hankinson and Lowesmith used the equations

originally developed for LNG with the equivalent mass of methane based on equal net energy (120 MJ/kg for H_2 and 50 MJ/kg for CH_4 → 1 kg H_2 is equivalent to 2.4 kg CH_4).

$$D\ (m) = A\ .\ M^{1/3}$$
$$H\ (m) = B\ .\ M^{1/3}$$
$$t\ (\text{duration in sec}) = C.\ M^{1/3}$$

It is interesting to note that the power dependence of this large diffusion flame is ⅓ compared to a power dependence of ⅛ generally observed for premixed processes as detonation, fast flame or high explosive.

However it has to be noticed that the maximum pressure of the storage is higher than the critical pressure of H_2 (P_c = 13 bars & T_c = 33 K). Hence, in case of failure, H_2 would be in supercritical conditions and then more as a gas forming a blast wave and a fireball.

Within the SafeLNG Dutch program, a large scale bonfire test was conducted by TNO in cooperation with the German BAM Institute in Berlin, where a double wall vacuum perlite insulated tank (3m^3) filled with LN_2 was exposed for about 2 hours to a heat stress experiment with heat loads of 75 kW/m^2. It was observed that the vacuum was lost and the outer tank showed restricted buckling but the perlite insulation maintained its performance and the inner tank never at any point showed temperatures above 50°C, well below the temperature of 300°C where the strength of the inner steel tank would start to deteriorate.

TNO concluded that a double-walled pressure tank is able to endure a long exposure to radiation intensities of 35 kW/m^2. For a full size LNG storage tank (45 m^3) with a much larger content, simulations show that it would take many hours (6-8) before the pressure relief valve would start venting.

Rapid Phase Transition RPT

Theoretically, there are 3 types of RPT events: spontaneous, delayed and triggered.

For spontaneous RPTs the following condition must be satisfied:

$$1.0 < T_w / T_{sl} < 1.1$$

where T_w is the water temperature (K) and T_{sl} (K) is the cryogen superheat limit temperature. To a good approximation,

$$T_{sl} = 0.89\ T_c$$

Where T_c is the critical temperature (K). Hence for spontaneous RPTs to occur,

$$0.9 < T_w / T_c < 1.0$$

Thus, if T_w is too low then there is insufficient temperature difference between the water and cryogen for nucleate boiling to maintain a high enough heat transfer rate required for RPT. If Tw is too high then again the heat transfer rate is insufficient because the heat transfer takes place in the film boiling regime. LH_2 has a T_c of 33 K, then spontaneous RPT is not possible.

Delayed RPTs occur when the liquid is composed of several components, such as LNG. As the methane preferentially evaporates from the pool with respect to the heavier hydrocarbons, T_{sl} rises and when the methane composition falls below about 40%, RPTs can readily occur. These are "delayed" RPTs. Clearly for pure liquid hydrogen these RPTs cannot happen (theoretically).

Triggered RPTs can occur when the vapour film which normally separates the liquid from the water in the stable film boiling regime is broken down by external forces to allow direct physical contact between the water and liquid. Examples of triggers are waves breaking over the liquid pool, momentum of falling liquid, deliberate use of explosives, or energy release from delayed RPTs elsewhere in the pool.

To our information, there is no LH_2 RPT experiments in the litterature. As a consequence, it would be interesting to investigate experimentally to see if LH_2 respects the theory and if the models of overpressure generation are valid.

4.4 Remaining knowledge gaps

Based on this literature survey, the knowledge gaps to be filled are :

- Flame acceleration and detonation properties of cold H_2/air mixtures,
- Flame propagation in heterogeneous cold mixtures on presence of obstacles.

Additional R&D activities on LH_2 jet and pool fire is not considered as a priority.

Due to budget limitation, RPT and BLEVE are not studied in this project. Nevertheless, these phenomena will be addressed in the framework of the SH2IFT Norway/Industry funded project. The results of the project will be published in open litterature.

5 General Conclusions

A literature survey on physics associated with liquid hydrogen hazards has been performed. This literature survey will be used in association with the PIRT (Phenomena Identification Ranking Table) planned in September 2018 at the Research Priorities Workshop (Buxton) to refine and improve the experimental and modelling program.